Hybrid Channel Coding for Error-Sensitive Class on DS-CDMA Air Interface

by

Byungwan Yu

Thesis submitted to the faculty of Virginia Polytechnic Institute and State University in partial fulfillment of the requirements for the degree of

Masters of Science
In
Electrical and Computer Engineering

Brian D. Woerner, Chairman
Jeffrey H. Reed
R. Mike Buehrer

August 2003
Blacksburg, Virginia

Keywords: hybrid, WCDMA, error-sensitive, ARQ, BCH, FEC

Hybrid Channel Coding for Error-Sensitive Class on DS-CDMA Air Interface

Byungwan Yu

(ABSTRACT)

A DS-CDMA system with QPSK modulation and a RAKE receiver is modeled and simulated. A mathematical description of the DS-CDMA system is provided on uplink and downlink. For a multipath channel environment, modeling techniques for AWGN and Rayleigh fading are illustrated. Comparisons are made concerning the performance of CDMA systems with hybrid data rates.

The thesis proposes a technique for hybrid channel coding for ARQ (Automatic-Repeat-reQuest) protocol and FEC (Forward Error Correction) scheme that can reduce the error rate significantly. Each of ARQ protocol and FEC scheme gives rise to long latency and significant complexity, respectively, for obtaining the required QoS (Quality of Service). This thesis shows using theoretical analysis and computer simulations that synergistic effects are possible by using both an ARQ protocol and a FEC scheme.

Acknowlegements

I would like to thank my advisor, Dr. Brian D. Woerner for his encouragement and counsel through this thesis. Without his help, it would not have been possible to complete this work. I would like to thank my committee members Dr. Reed and Dr. Buehrer for their corrections and comments on this thesis.

I would also like to thank Hae-Soo Kim and Kyung-Kyoon Bae for their valuable assistance and their friendship.

Finally, this work is dedicated to my parents for their everlasting love and support.

Contents

List of Tables

List of Figures

Chapter 1. Introduction

WCDMA (Wideband Code Division Multiple Access) technology is a widely adopted third generation air interface. A key difference between second generation IS-95 system and WCDMA is that packet data is supported for high data rate. This means that the cellular phone is not just a wireless phone any more, but a host supporting networking. Packet data in WCDMA are classified according to applications; for example, videotelephony, video games, streaming multimedia, web browsing and email. Also, they require different quality of service (QoS) which is one of most important challenges in WCDMA [14].

Therefore, as shown in Table 1-1, there are four kinds of traffic classes: conversational class, streaming class, interactive class and background.

Table 1-1. WCDMA QoS classes

Traffic class	Conversational class	Streaming class	Interactive class	Background
Example of the application	voice, videotelephony, video games	streaming multimedia	web browsing, network games	background download of emails

Clearly, some of these classes of data may be considered error sensitive, while others may be considered delay sensitive, and others both. In WCDMA, the bundle of error-sensitive data is treated as well as delay-sensitive data. Powerful error control schemes may be important for error-sensitive data.

1.1 Multiple Access Scheme

While many first and second generation systems relied on Time Division Multiple Access (TDMA) or Frequency Division Multiple Access (FDMA), most third generation systems will be based on Code Division Multiple Access (CDMA). CDMA users are assigned their own spreading code to simultaneously communicate with other users, since frequency resources are limited compared to countless potential users. The goal of International Mobile Telephony 2000 (IMT-2000) is to establish the united core network of several different regional air interfaces defined for third generation Mobile communication systems [14]. As shown in Figure 1-1, WCDMA is one kind of air interfaces associated with IMT-2000.

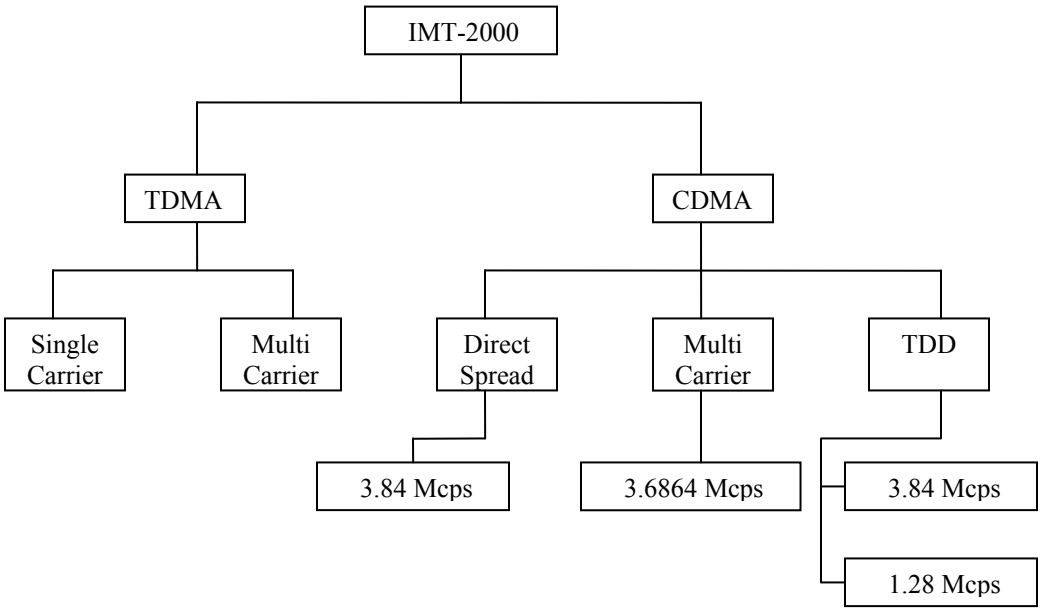

Figure 1-1. IMT-2000 air interfaces

IS-95 is a standard for the second generation air interface. The main differences between IS-95 and WCDMA are useable bandwidth and synchronicity of base stations. In WCDMA, the bandwidth is 5 MHz per channel instead of 1.25 MHz per channel for IS-95. Larger bandwidth can support higher data rate. The chip rate of WCDMA is 3.84 Mcps compared to 1.2288 Mcps for IS-95. Moreover, in WCDMA, different data rates may be simultaneously supported using Orthogonal Variable Spreading Factor (OVSF) code assignment. So advanced radio resource management algorithms are necessary to guarantee quality of service and to maximize system throughput [14]. Also, the base stations of WCDMA are asynchronous. Therefore, the synchronization from GPS is unnecessary.

In this thesis, the considered transceiver system is based on WCDMA parameters, including a carrier frequency of 2 GHz, a chip rate of 3.84 Mcps, and the OVSF codes for spreading. However, the primary purpose of this thesis is not to exactly model the WCDMA interface but rather to explore performance tradeoffs with a CDMA system with variable data rates.

1.2 Purpose of Research

Within a CDMA system, the processing gain provides some protect against noise, fading, and interference. However, within a variable data rate system with some users operating at high data rates and low processing gain, the processing gain by itself may be insufficient to insure data integrity. Other schemes are needed to decrease the probability of bit errors. Usually, channel coding and diversity cooperate to lower the error probability. To obtain the coding gain, the code word from the encoder of transmitter is

decoded at receiver. The weakness of channel coding is that redundant bits lead to a decrease of information bit rate, and increase of hardware complexity.

On the other hand, the temporal and spatial diversity gain can be used to enhance receiver performance. For instance, the RAKE receiver maximizes the signal-to-interference (SIR) ratio by absorbing multipath signals with different time intervals, and beamforming at the antenna exploits the direction of desired signals for maximum SIR.

This thesis is focused on the channel coding scheme. The hybrid use of the automatic-repeat-request (ARQ) protocol and forward error correction (FEC) scheme is investigated. Normally FEC is traditionally used by itself. In the ARQ scheme, the receiver detects erroneous code words and requests the retransmission for an erroneous code word. The ARQ scheme can be used unless all retransmitted code words are always erroneous due to an irreducible error floor. As the probability of error code word becomes lower or the maximum number of retransmissions for an erroneous code word becomes larger, the coding gain from the ARQ scheme increases. The FEC can play a role in decreasing the probability of codeword error. Therefore, a synergistic effect is achieved from the hybrid use of the two error control techniques. A similar study is accomplished in the recent work of V.R. de Carvalho and C. de Almeida. However, the uniqueness of this thesis is that the FEC is used before requesting a retransmission.

1.3 Outline of Thesis

This thesis consists of five chapters. The primary means of verifying theoretical analysis are through computer simulations. The essential system is a DS-CDMA transceiver in which the QPSK modulation scheme and a 3-finger RAKE receiver are used.

Chapter 2 describes the DS-CDMA transceiver from a mathematical view. The uplink and downlink portions are included.

Chapter 3 describes how the CDMA system is simulated. It explains the procedure for generating AWGN, frequency selective channel and spreading codes.

In Chapter 4, the simulation results for ARQ, FEC and the hybrid scheme are provided, and compared. Also, a theoretical upper bound on performance is present.

Chapter 5 concludes this thesis and offers directs for future work.

Chapter 2. DS-CDMA transceiver

In this thesis, we consider the analysis of Direct-Sequence Code Division Multiple Access (DS-CDMA) systems with mixed-data rates. In particular, we are interested in understanding the performance of hybrid error control schemes for these systems. In this chapter, we define a system model that we will employ throughout the thesis.

2.1. Transmitter

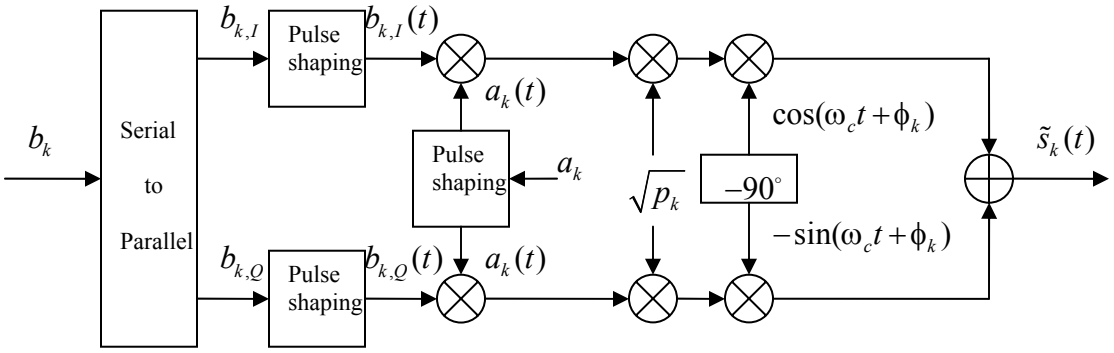

Figure 2-1. Transmitter

Figure 2-1 presents a block diagram of a DS-CDMA transmitter. The data bits $\{b_k\}$ for the k^{th} user are transmitted after spreading and QPSK modulation. For each of in-phase and quadrature component, BPSK spreading is used. The data bits $\{b_k\}$ are randomly generated, and assumed independent and identically distributed. $\tilde{s}_k(t)$ denotes the transmitted signal of k^{th} user and is mathematically represented by

$$\tilde{s}_k(t) = \mathrm{Re}\left\{\left(\sqrt{p_k}b_{k,I}(t)a_k(t) + j\sqrt{p_k}b_{k,Q}(t)a_k(t)\right)e^{j(\omega_c t+\phi_k)}\right\} \quad (2\text{-}1)$$

$$= \mathrm{Re}\left\{s_k(t)e^{j\omega_c t}\right\}, \quad (2\text{-}2)$$

where $s_k(t)$ is the complex baseband representation of the transmitted signal $\tilde{s}_k(t)$ and given by

$$s_k(t) = \left(\sqrt{p_k}b_{k,I}(t)a_k(t) + j\sqrt{p_k}b_{k,Q}(t)a_k(t)\right)e^{j\phi_k} \quad (2\text{-}3)$$

where $\sqrt{p_k}$ is the normalized power of k^{th} user and ϕ_k is the phase of carrier signal for k^{th} user. After serial to parallel conversion of the data stream, $b_{k,I}(t)$ and $b_{k,Q}(t)$ are the data signals of in-phase branch and quadrature branch respectively, and expressed as

$$b_{k,I}(t) = \sum_{i=-\infty}^{\infty} b_{k,I}^{(i)} p_{T_b}(t - iT_b), \quad (2\text{-}4)$$

and

$$b_{k,Q}(t) = \sum_{i=-\infty}^{\infty} b_{k,Q}^{(i)} p_{T_b}(t - iT_b), \quad (2\text{-}5)$$

where $b_{k,I}^{(i)}$ and $b_{k,Q}^{(i)} \in \{\pm 1\}$ are the i^{th} bit of the k^{th} user for the in-phase and quadrature branches respectively. The signal pulse $p_{T_b}(t)$ is a unit rectangular pulse defined by

$$p_{T_b} = \begin{cases} 1 & if \;\; 0 \le t < T_b \\ 0 & elsewhere \end{cases}. \quad (2\text{-}6)$$

T_b is the duration of one bit. In Equation (2-3), $a_k(t)$ is a spreading waveform and can be written by

$$a_k(t) = \sum_{j=-\infty}^{\infty} a_k^{(j)} p_{T_c}(t - jT_c) \quad (2\text{-}7)$$

where $a_k^{(j)} \in \{\pm 1\}$ is the j^{th} chip of the k^{th} user's spreading sequence $\{a_k^{(j)}\}$, and $p_{T_c}(t)$ is a unit rectangular pulse defined by

$$p_{T_c} = \begin{cases} 1 & if \ \ 0 \le t < T_c \\ 0 & \ \ elsewhere \end{cases}. \tag{2-8}$$

While most commercial system use non-rectangular pulse shaping for the spreading sequences, our study focus primarily on the interaction of CDMA signals of different data rates, which will not be greatly affected by the choice of pulse waveform. Therefore we use rectangular pulses for simplicity.

2.2. Multipath Channel

In a wireless channel, the signal is propagated in all direction with omni-directional antenna or through given range of angles with a sectorized antenna. Because of the presence of obstructions and reflectors in the wireless environment, multiple copies of the transmitted signal are received at the receiver with different time delay and different amplitude fading due to reflection against various objects on the channel. These arriving signals experience different paths. In other words, assuming a channel as a linear time-variant filter, each multipath signal passes through its own channel filter with different coefficients. The impulse response of the multipath fading channel can be represented as

$$\tilde{h}(t,\tau) = \mathrm{Re}\left\{h(t,\tau)e^{j\omega_c t}\right\} \tag{2-9}$$

where τ is a multipath delay and ω_c is a carrier angle frequency. The signal $h(t,\tau)$ is the complex baseband impulse response and expressed for k^{th} user as

$$h_k(t,\tau) = \sum_{l=1}^{L} \alpha_{k,l} e^{j\varphi_{k,l}} \delta(t - \tau_{k,l}), \qquad k = 1, 2, \cdots, K \qquad (2\text{-}10)$$

where L : Number of multipath components;

$\alpha_{k,l}$: Amplitude fading of l^{th} path (Rayleigh distributed random variable);

$\tau_{k,l}$: Delay of l^{th} path;

$\varphi_{k,l}$: Phase shift of l^{th} path (uniform distributed random variable);

$\delta(\cdot)$: Dirac delta function,

and the subscript k exists to represent k^{th} user.

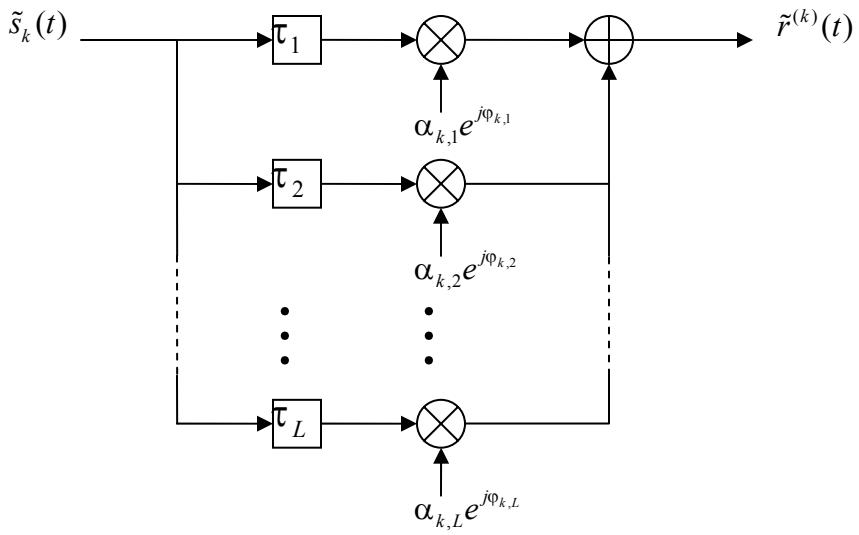

Figure 2-2. Multipath channel with L paths

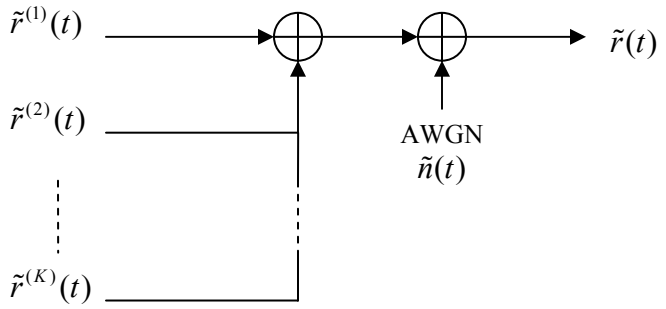

Figure 2-3. Received signal with K users

As shown in Figure 2-2, the number of multipath is assumed as L, and each path is with different delay and fading. Figure 2-3 depicts that the received signal $\tilde{r}(t)$ is a sum of all multipath signals of all users and the additive white Gaussian noise (AWGN). The received signal in baseband form can be written by

$$r(t) = n(t) + \frac{1}{2}\sum_{k=1}^{K} s_k(t) * h_k(t) \tag{2-11}$$

where $(*)$ symbolizes convolution of two sequences and $n(t)$ is an complex baseband expression of the AWGN with two-sided power spectral density $s_n(f) = \frac{N_0}{2}$. The noise can be expressed in passband form as

$$\tilde{n}(t) = \mathrm{Re}\left\{ n(t) e^{j\omega_c t} \right\} \tag{2-12}$$

The factor of $1/2$ in Equation (2-11) is due to the properties of the complex envelope, in order to represent the passband radio system at baseband [7].

2.3. Receiver

Figure 2-4 depicts a single-user Rake receiver, assuming that perfect channel estimation is carried out. The Rake receiver has M fingers which demodulate each multipath signal, using a correlation receiver as shown in Figure 2-5. In Figure 2-5, the index $l^{(m)}$ refers to the l^{th} strongest component locked onto by the m^{th} correlation branch. The Rake receiver can use either Maximal Ratio Combining (MRC) or Equal Gain Combining as a temporal diversity combining technique. In Figure 2-5, MRC is used and the weight $\alpha_{k,l^{(m)}}$ is the complex conjugate of the corresponding channel tap coefficient.

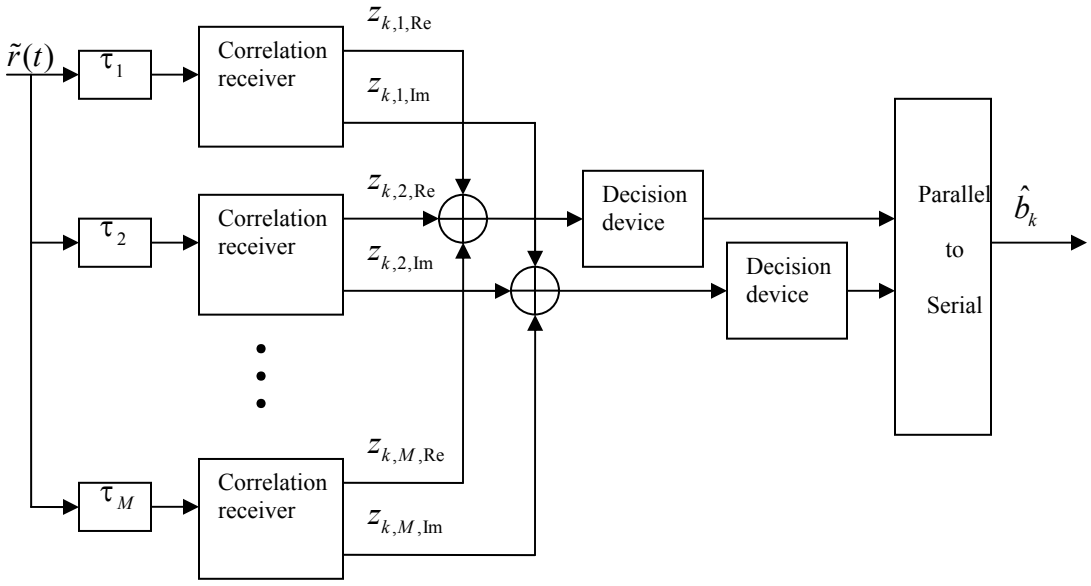

Figure 2-4. Rake receiver (M fingers)

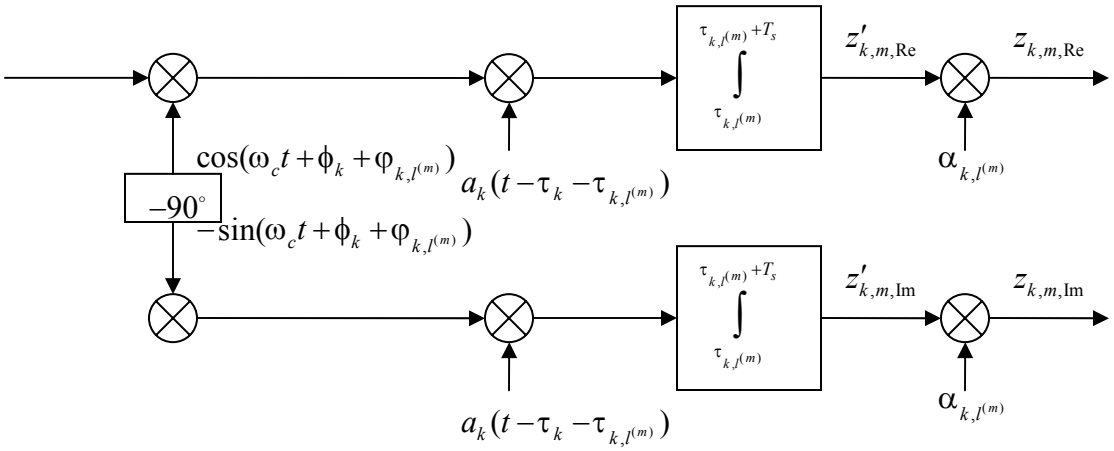

Figure 2-5. Correlation receiver (m^{th} branch)

The received signal is separated into the in-phase and quadrature baseband signal by multiplying sinusoidal carriers, $\cos(\omega_c t+\phi_k+\varphi_{k,l^{(m)}})$ and $-\sin(\omega_c t+\phi_k+\varphi_{k,l^{(m)}})$ respectively. Assuming that the receiver is coherent, the phase shift ϕ_k of k^{th} user is known at the receiver. Equivalently the demodulation process can be modeled for complex envelope representation by multiplying $e^{-j\varphi_{k,l}}$ to each l^{th} path signal of k^{th} user in complex baseband form. Since it is assumed that acquisition and time tracking are perfectly achieved, it is assumed that phase tracking is conducted prior to dispreading in Figure 2-5. The baseband signal is despreaded with the signature waveform $a_k(t-\tau_k-\tau_{k,l^{(m)}})$. Finally, all outputs from each finger are combined by weighting by the amplitude of the complex channel coefficient, $\alpha_{k,l^{(m)}}$. The decision device yields estimated data bits from the combined decision statistic. At the end of the receiver, the in-phase and quadrature bits are combined into a sequence of estimated data bits.

To this point, the discussion applied equally to the uplink and downlink portions of a DS-CDMA cellular system. One key difference between the uplink and downlink is the ability to support synchronous transmission. Since signals on the uplink originate at mobile handsets on different locations, it is generally not possible to synchronize these transmissions down to the data bit level. The resulting timing of multiple signals on the uplink is illustrated in Figure 2-6.

For downlink signal that all originate at a common transmitter location, it is possible to achieve bit synchronization for the first arriving component in the signals. However, multiple may still cause overlap between consecutive signal bits as illustrated in Figure 2-7.

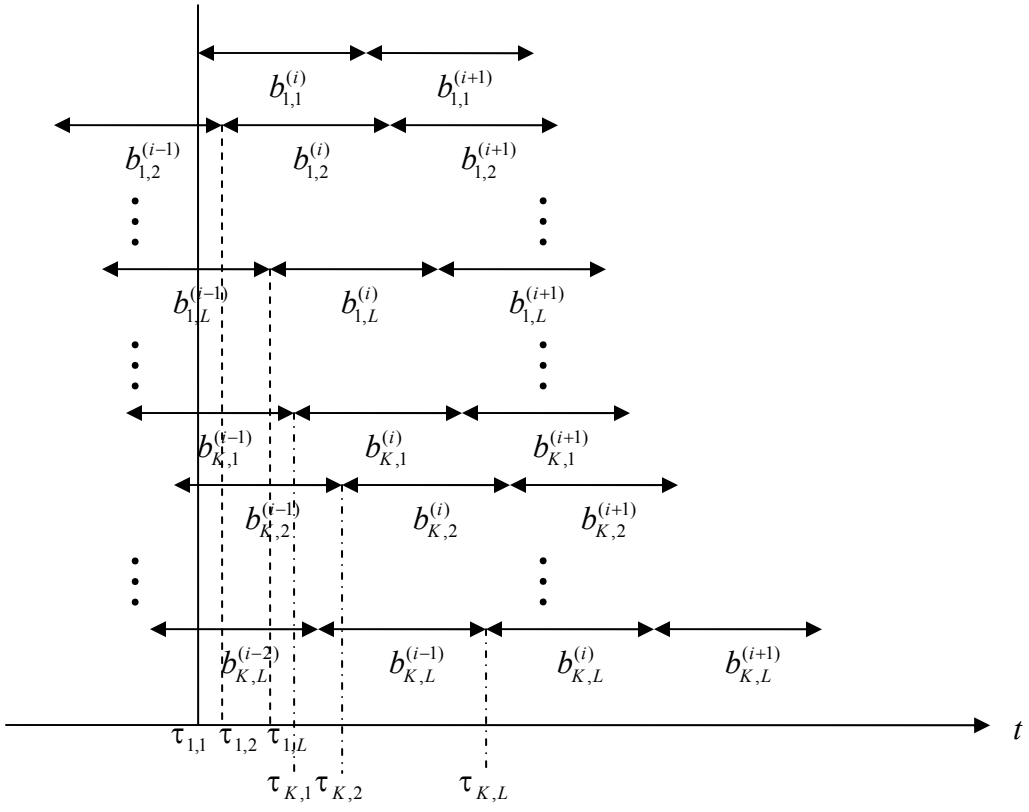

Figure 2-6. Asynchronously transmitted signals (Uplink)

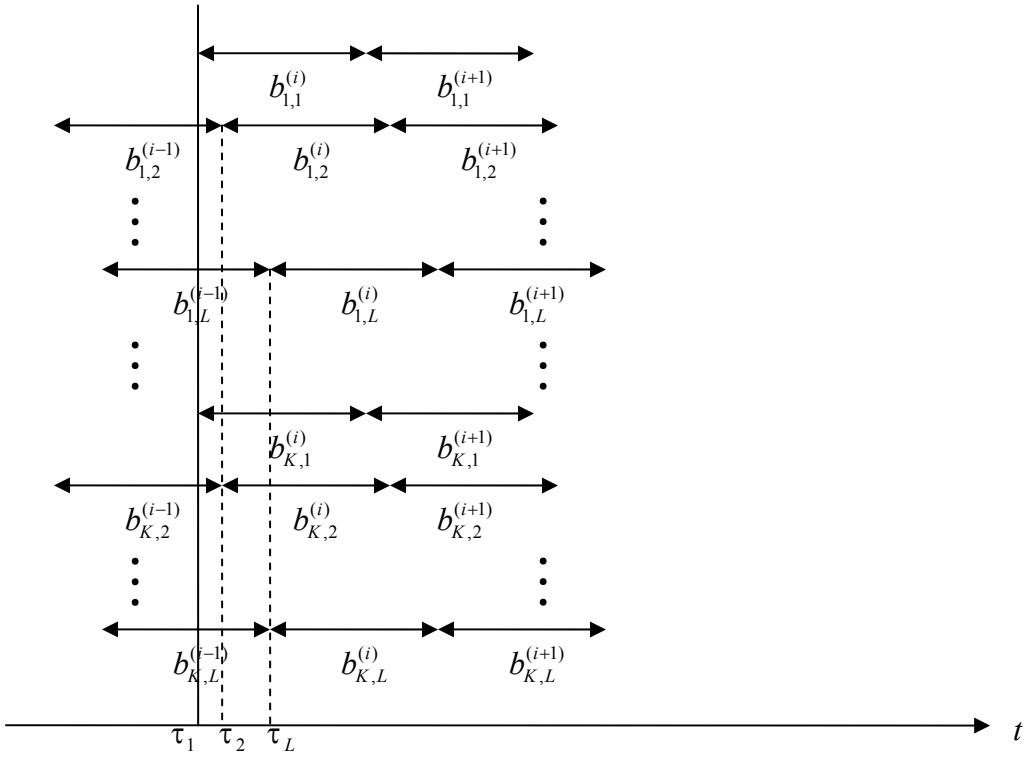

Figure 2-7. Synchronously transmitted signals (Downlink)

In Figure 2-6, $\tau_{k,l}$ denotes the l^{th} path delay of the k^{th} user. Since each signal originates at a different location, the multipath profile for each user will be different. Each arriving data bit will overlap with multiple data bits of interfering users, producing a complicated mix of multiple access and multipath interference.

In the synchronous case of Figure 2-7, all users signal undergo the same multipath channel (i.e., $\tau_{k,l} = \tau_l$, for $k = 1, 2, \cdots, K$). $b_{k,l}^{(i)}$ denotes i^{th} bit on the l^{th} path of k^{th} user. Note that individual arriving components from each user align at start and finish times, although multipath delays can result in multiple access interference between overlapping bits of different users.

The received signal is a sum of user signals, their multipath delayed signals and the AWGN. From Equation (2-3) and (2-10), the received signal for the asynchronous (uplink) case can be expressed as

$$r_a(t) = n(t) + \frac{1}{2}\sum_{k=1}^{K}\sum_{l=1}^{L}\alpha_{k,l}s_k(t-\tau_k-\tau_{k,l})e^{j\varphi_{k,l}} \ . \tag{2-13}$$

In the synchronous (downlink) case, the received signal can be expressed as

$$r_s(t) = n(t) + \frac{1}{2}\sum_{k=1}^{K}\sum_{l=1}^{L}\alpha_{l}s_k(t-\tau_l)e^{j\varphi_{l}} \ . \tag{2-14}$$

In cellular CDMA system, all transmitted signals are combined synchronously on downlink from a base station to mobile users. On the other hand, all transmitted signals are combined asynchronously on uplink from mobile users to a base station. The uplink and downlink are separated by using different frequency bands or different time slots (i.e., frequency division duplex (FDD) or time division duplex (TDD)). In Equation (2-13), τ_k denotes the parameter for the relative random delay of the k^{th} user's signal to the first arriving signal. Equation (2-3) is substituted into Equation (2-13) as follows:

$$\begin{aligned} r_a(t) = n(t) + \frac{1}{2}\sum_{k=1}^{K}\sum_{l=1}^{L}\alpha_{k,l}\{&\sqrt{p_k}b_{k,I}(t-\tau_k-\tau_{k,l})a_k(t-\tau_k-\tau_{k,l}) \\ &+ j\sqrt{p_k}b_{k,Q}(t-\tau_k-\tau_{k,l})a_k(t-\tau_k-\tau_{k,l})\}e^{j\theta_{k,l}} \end{aligned} \tag{2-15}$$

In Equation (2-15), $\theta_{k,l}$ is equal to $\phi_k + \varphi_{k,l}$ and denotes the phase shift of the k^{th} user's l^{th} multipath component at the receiver.

The bandpass waveform of the asynchronous received signal $r_a(t)$ can be written as

$$\tilde{r}_a(t) = \mathrm{Re}\{r_a(t)e^{j\omega_c t}\} \ . \tag{2-16}$$

For the sake of simplicity, the in-phase term and quadrature term in Equation (2-15) are expressed as follows:

$$In_{k,l} = \sqrt{p_k} b_{k,I}(t-\tau_k-\tau_{k,l}) a_k(t-\tau_k-\tau_{k,l}) \tag{2-17}$$

$$Qu_{k,l} = \sqrt{p_k} b_{k,Q}(t-\tau_k-\tau_{k,l}) a_k(t-\tau_k-\tau_{k,l}) \tag{2-18}$$

From Equation (2-17) and (2-18), Equation (2-16) can be written as

$$\begin{aligned}\tilde{r}_a(t) &= \mathrm{Re}\{n(t)e^{j\omega_c t} + \frac{1}{2}\sum_{k=1}^{K}\sum_{l=1}^{L}\alpha_{k,l}(In_{k,l}+jQu_{k,l})e^{j(\omega_c t+\theta_{k,l})}\} \\ &= \mathrm{Re}[n(t)e^{j\omega_c t} + \frac{1}{2}\sum_{k=1}^{K}\sum_{l=1}^{L}\alpha_{k,l}\{(In_{k,l}\cos(\omega_c t+\theta_{k,l}) - Qu_{k,l}\sin(\omega_c t+\theta_{k,l})) \\ &\quad + j(In_{k,l}\sin(\omega_c t+\theta_{k,l}) + Qu_{k,l}\cos(\omega_c t+\theta_{k,l}))\}] \\ &= \tilde{n}(t) + \frac{1}{2}\sum_{k=1}^{K}\sum_{l=1}^{L}\alpha_{k,l}\{In_{k,l}\cos(\omega_c t+\theta_{k,l}) - Qu_{k,l}\sin(\omega_c t+\theta_{k,l})\}.\end{aligned} \tag{2-19}$$

As shown in Figure 2-4, the m^{th} finger of the Rake receiver grabs the m^{th} strongest signal of the multipath arriving signals. Assuming that $\theta_{k,l}$ and $\alpha_{k,l}$ are known from channel estimation, the decision statistic $z'_{k,m}$ from the m^{th} correlator branch can be represented by

$$\begin{aligned}z'_{k,m,\mathrm{Re}} &= \int_{\tau_{k,l^{(m)}}}^{\tau_{k,l^{(m)}}+T_s} \tilde{r}_a(t)\{\cos(\omega_c t+\theta_{k,l^{(m)}})a_k(t-\tau_k-\tau_{k,l^{(m)}})\}dt \\ &= \int_{\tau_{k,l^{(m)}}}^{\tau_{k,l^{(m)}}+T_s} [\{\tilde{n}(t) + \frac{1}{2}\sum_{k'=1}^{K}\sum_{l=1}^{L}\alpha_{k',l}(In_{k',l}\cos(\omega_c t+\theta_{k',l}) \\ &\qquad - Qu_{k',l}\sin(\omega_c t+\theta_{k',l}))\}\{\cos(\omega_c t+\theta_{k,l^{(m)}})a_k(t-\tau_k-\tau_{k,l^{(m)}})\}]dt,\end{aligned} \tag{2-20}$$

and

$$z'_{k,m,\mathrm{Im}} = \int_{\tau_{k,l^{(m)}}}^{\tau_{k,l^{(m)}}+T_s} \tilde{r}_a(t)\{-\sin(\omega_c t+\theta_{k,l^{(m)}})a_k(t-\tau_k-\tau_{k,l^{(m)}})\}dt$$

$$= \int_{\tau_{k,l^{(m)}}}^{\tau_{k,l^{(m)}}+T_s} [\{\tilde{n}(t) + \frac{1}{2}\sum_{k'=1}^{K}\sum_{l=1}^{L}\alpha_{k',l}(In_{k',l}\cos(\omega_c t + \theta_{k',l}) - Qu_{k',l}\sin(\omega_c t + \theta_{k',l}))\}\{-\sin(\omega_c t + \theta_{k,l^{(m)}})a_k(t - \tau_k - \tau_{k,l^{(m)}})\}]dt, \quad (2\text{-}21)$$

where T_s is the symbol duration of the QPSK modulated signal and k' is the user index varying from 1 to K. K is the total number of users. Equations (2-20) and (2-21) can each be separated into three components: noise, desired signal component and interference. The interference is caused by the other users and other multipaths.

Therefore, the decision statistic can be represented by

$$z'_{k,m,\mathrm{Re}} = \xi_I + A_I + \sum_{\substack{l=1 \\ l\neq l^{(m)}}}^{L} I_{k,l,\mathrm{Re}} + \sum_{\substack{k'=1 \\ k'\neq k}}^{K}\sum_{l=1}^{L} I_{k',l,\mathrm{Re}}\,, \quad (2\text{-}22)$$

and

$$z'_{k,m,\mathrm{Im}} = \xi_Q + A_Q + \sum_{\substack{l=1 \\ l\neq l^{(m)}}}^{L} I_{k,l,\mathrm{Im}} + \sum_{\substack{k'=1 \\ k'\neq k}}^{K}\sum_{l=1}^{L} I_{k',l,\mathrm{Im}}\,, \quad (2\text{-}23)$$

where ξ_I and ξ_Q symbolize the contribution of the Gaussian noise $\tilde{n}(t)$ in the in-phase component and the quadrature component. Each of ξ_I and ξ_Q has zero mean and variance $\frac{N_0 T_s}{4}$, and are defined by

$$\xi_I = \int_{\tau_{k,l^{(m)}}}^{\tau_{k,l^{(m)}}+T_s} \tilde{n}(t)\{\cos(\omega_c t + \theta_{k,l^{(m)}})a_k(t - \tau_k - \tau_{k,l^{(m)}})\}dt\,, \quad (2\text{-}24)$$

and

$$\xi_Q = \int_{\tau_{k,l^{(m)}}}^{\tau_{k,l^{(m)}}+T_s} \tilde{n}(t)\{-\sin(\omega_c t + \theta_{k,l^{(m)}})a_k(t - \tau_k - \tau_{k,l^{(m)}})\}dt\,. \quad (2\text{-}25)$$

The term A_I and A_Q represent the in-phase and quadrature contribution of the desired component to the overall decision statistic. The desired component can be written as

$$A_I = \int_{\tau_{k,l^{(m)}}}^{\tau_{k,l^{(m)}}+T_s} \frac{1}{2}\sqrt{p_k}\alpha_{k,l^{(m)}}[\{b_{k,I}(t-\tau_k-\tau_{k,l^{(m)}})\cos(\omega_c t+\theta_{k,l^{(m)}})-b_{k,Q}(t-\tau_k-\tau_{k,l^{(m)}}) \cdot \sin(\omega_c t+\theta_{k,l^{(m)}})\}a_k(t-\tau_k-\tau_{k,l^{(m)}})\cos(\omega_c t+\theta_{k,l^{(m)}})a_k(t-\tau_k-\tau_{k,l^{(m)}})]dt \quad (2\text{-}26)$$

and

$$A_Q = \int_{\tau_{k,l^{(m)}}}^{\tau_{k,l^{(m)}}+T_s} \frac{1}{2}\sqrt{p_k}\alpha_{k,l^{(m)}}[\{b_{k,I}(t-\tau_k-\tau_{k,l^{(m)}})\cos(\omega_c t+\theta_{k,l^{(m)}})-b_{k,Q}(t-\tau_k-\tau_{k,l^{(m)}}) \cdot \sin(\omega_c t+\theta_{k,l^{(m)}})\}a_k(t-\tau_k-\tau_{k,l^{(m)}})(-1)\sin(\omega_c t+\theta_{k,l^{(m)}})a_k(t-\tau_k-\tau_{k,l^{(m)}})]dt \quad (2\text{-}27)$$

for the m^{th} finger of k^{th} user. After integrating these expression over the symbol duration, the term $b_{k,I}(t-\tau_k-\tau_{k,l^{(m)}})$ yields $b_{k,I}^i$ which is the i^{th} bit of in-phase data bits, and the term $b_{k,Q}(t-\tau_k-\tau_{k,l^{(m)}})$ yields $b_{k,Q}^i$ which is the i^{th} bit of quadrature data bits. Thus A_I and A_Q are found to be

$$A_I = \frac{1}{4}\sqrt{p_k}\alpha_{k,l^{(m)}}b_{k,I}^i T_s, \quad (2\text{-}28)$$

and

$$A_Q = \frac{1}{4}\sqrt{p_k}\alpha_{k,l^{(m)}}b_{k,Q}^i T_s. \quad (2\text{-}29)$$

As shown in Equation (2-28) and (2-29) derived from Equation (2-26) and (2-27), the in-phase component and quadrature component do not affect each other since they are orthogonal.

The other terms in Equation (2-22) and (2-23) are the interference except ξ_I, ξ_Q, A_I and A_Q. The $(m-1)$ copies of the desired signal arrive at the Rake receiver with time

differences and interfere with the desired m^{th} multipath component. This interference can be written as

$$I_{k,l,\mathrm{Re}} = \int_{\tau_{k,l^{(m)}}}^{\tau_{k,l^{(m)}}+T_s} \frac{1}{2}\sqrt{p_k}\alpha_{k,l}[\{b_{k,I}(t-\tau_k-\tau_{k,l})\cos(\omega_c t+\theta_{k,l}) - b_{k,Q}(t-\tau_k-\tau_{k,l}) \cdot \sin(\omega_c t+\theta_{k,l})\}a_k(t-\tau_k-\tau_{k,l})\cos(\omega_c t+\theta_{k,l^{(m)}})a_k(t-\tau_k-\tau_{k,l^{(m)}})]dt$$

$$= \frac{1}{4}\sqrt{p_k}\alpha_{k,l}[\{\cos(\theta_{k,l}-\theta_{k,l^{(m)}})\times \int_{\tau_{k,l^{(m)}}}^{\tau_{k,l^{(m)}}+T_s} b_{k,I}(t-\tau_k-\tau_{k,l})a_k(t-\tau_k-\tau_{k,l}) \cdot a_k(t-\tau_k-\tau_{k,l^{(m)}})dt\} - \{\sin(\theta_{k,l}-\theta_{k,l^{(m)}})\times \int_{\tau_{k,l^{(m)}}}^{\tau_{k,l^{(m)}}+T_s} b_{k,Q}(t-\tau_k-\tau_{k,l}) \cdot a_k(t-\tau_k-\tau_{k,l})a_k(t-\tau_k-\tau_{k,l^{(m)}})dt\}], \quad (2\text{-}30)$$

and

$$I_{k,l,\mathrm{Im}} = \int_{\tau_{k,l^{(m)}}}^{\tau_{k,l^{(m)}}+T_s} \frac{1}{2}\sqrt{p_k}\alpha_{k,l}[\{b_{k,I}(t-\tau_k-\tau_{k,l})\cos(\omega_c t+\theta_{k,l}) - b_{k,Q}(t-\tau_k-\tau_{k,l}) \cdot \sin(\omega_c t+\theta_{k,l})\}a_k(t-\tau_k-\tau_{k,l})(-1)\sin(\omega_c t+\theta_{k,l^{(m)}})a_k(t-\tau_k-\tau_{k,l^{(m)}})]dt$$

$$= \frac{1}{4}\sqrt{p_k}\alpha_{k,l}[\{(-1)\sin(\theta_{k,l}-\theta_{k,l^{(m)}})\times \int_{\tau_{k,l^{(m)}}}^{\tau_{k,l^{(m)}}+T_s} b_{k,I}(t-\tau_k-\tau_{k,l})a_k(t-\tau_k-\tau_{k,l}) \cdot a_k(t-\tau_k-\tau_{k,l^{(m)}})dt\} + \{\cos(\theta_{k,l}-\theta_{k,l^{(m)}})\times \int_{\tau_{k,l^{(m)}}}^{\tau_{k,l^{(m)}}+T_s} b_{k,Q}(t-\tau_k-\tau_{k,l}) \cdot a_k(t-\tau_k-\tau_{k,l})a_k(t-\tau_k-\tau_{k,l^{(m)}})dt\}], \quad (2\text{-}31)$$

where the interference $I_{k,l,\mathrm{Re}}$ to the in-phase component and the interference $I_{k,l,\mathrm{Im}}$ to the quadrature component are caused by the l^{th} multipath component of the k^{th} desired user (i.e., $k' = k$ and $l \neq l^{(m)}$). Moreover, the decision statistic includes the other interference term caused by all the multipath signals of the other users, which may be expressed as

$$I_{k',l,\mathrm{Re}} = \int_{\tau_{k,l^{(m)}}}^{\tau_{k,l^{(m)}}+T_s} \frac{1}{2}\sqrt{p_{k'}}\alpha_{k',l}[\{b_{k',I}(t-\tau_{k'}-\tau_{k',l})\cos(\omega_c t+\theta_{k',l}) - b_{k',Q}(t-\tau_{k'}-\tau_{k',l})$$
$$\cdot\sin(\omega_c t+\theta_{k',l})\}a_{k'}(t-\tau_{k'}-\tau_{k',l})\cos(\omega_c t+\theta_{k,l^{(m)}})a_k(t-\tau_k-\tau_{k,l^{(m)}})]dt$$

$$= \frac{1}{4}\sqrt{p_{k'}}\alpha_{k',l}[\{\cos(\theta_{k',l}-\theta_{k,l^{(m)}})\times \int_{\tau_{k,l^{(m)}}}^{\tau_{k,l^{(m)}}+T_s} b_{k',I}(t-\tau_{k'}-\tau_{k',l})a_{k'}(t-\tau_{k'}-\tau_{k',l})$$
$$\cdot a_k(t-\tau_k-\tau_{k,l^{(m)}})dt\} - \{\sin(\theta_{k',l}-\theta_{k,l^{(m)}})\times \int_{\tau_{k,l^{(m)}}}^{\tau_{k,l^{(m)}}+T_s} b_{k',Q}(t-\tau_{k'}-\tau_{k',l}) \qquad (2\text{-}32)$$
$$\cdot a_{k'}(t-\tau_{k'}-\tau_{k',l})a_k(t-\tau_k-\tau_{k,l^{(m)}})dt\}]$$

for the in-phase decision statistic, and

$$I_{k',l,\mathrm{Im}} = \int_{\tau_{k,l^{(m)}}}^{\tau_{k,l^{(m)}}+T_s} \frac{1}{2}\sqrt{p_{k'}}\alpha_{k',l}[\{b_{k',I}(t-\tau_{k'}-\tau_{k',l})\cos(\omega_c t+\theta_{k',l}) - b_{k',Q}(t-\tau_{k'}-\tau_{k',l})$$
$$\cdot\sin(\omega_c t+\theta_{k',l})\}a_{k'}(t-\tau_{k'}-\tau_{k',l})(-1)\sin(\omega_c t+\theta_{k,l^{(m)}})a_k(t-\tau_k-\tau_{k,l^{(m)}})]dt$$

$$= \frac{1}{4}\sqrt{p_{k'}}\alpha_{k',l}[\{(-1)\sin(\theta_{k',l}-\theta_{k,l^{(m)}})\times \int_{\tau_{k,l^{(m)}}}^{\tau_{k,l^{(m)}}+T_s} b_{k',I}(t-\tau_{k'}-\tau_{k',l})a_{k'}(t-\tau_{k'}-\tau_{k',l})$$
$$\cdot a_k(t-\tau_k-\tau_{k,l^{(m)}})dt\} + \{\cos(\theta_{k',l}-\theta_{k,l^{(m)}})\times \int_{\tau_{k,l^{(m)}}}^{\tau_{k,l^{(m)}}+T_s} b_{k',Q}(t-\tau_{k'}-\tau_{k',l}) \qquad (2\text{-}33)$$
$$\cdot a_{k'}(t-\tau_{k'}-\tau_{k',l})a_k(t-\tau_k-\tau_{k,l^{(m)}})dt\}]$$

for the quadrature decision statistic, where $k' \neq k$.

From the M correlation receivers, M decision statistics are obtained. Within the Rake receiver, all the decision statistics are combined with appropriate weights. The weight represents how strong the corresponding multipath component and is obtained from channel estimation. Therefore, the final decision statistic can be expressed as

$$z_{k,\mathrm{Re}} = \sum_{m=1}^{M}\alpha_{k,m}z'_{k,m,\mathrm{Re}} \qquad (2\text{-}34)$$

for the in-phase part and

$$z_{k,\mathrm{Im}} = \sum_{m=1}^{M} \alpha_{k,m} z'_{k,m,\mathrm{Im}} \tag{2-35}$$

for the quadrature part where $\alpha_{k,m}$ is the amplitude of the complex channel coefficient. The reason why $\alpha_{k,m}$ is chosen for the weight is that it represents the relative strength of the m^{th} multipath component, and if interference can be modeled as Gaussian distributed leads to the optimum signal-to-noise ratio for the resulting decision statistic [7]. In the case of a perfect channel estimation, the weight is equal to $\alpha_{k,m}$.

Finally, the bit estimates are determined from the estimate $z_{k,\mathrm{Re}}$ and $z_{k,\mathrm{Im}}$ by the following decision rule

$$\hat{b}_{k,I}^{i} = \begin{cases} 1 & if \quad z_{k,\mathrm{Re}} \geq 0 \\ -1 & if \quad z_{k,\mathrm{Re}} < 0 \end{cases} \tag{2-36}$$

and

$$\hat{b}_{k,Q}^{i} = \begin{cases} 1 & if \quad z_{k,\mathrm{Im}} \geq 0 \\ -1 & if \quad z_{k,\mathrm{Im}} < 0 \end{cases} \tag{2-37}$$

where $\hat{b}_{k,I}^{i}$ and $\hat{b}_{k,Q}^{i}$ refer to the i^{th} bit estimate of the k^{th} user in the in-phase signal portion and that in the quadrature portion respectively. To obtain serial bit estimates, the in-phase bits and the quadrature bits are combined as shown in Figure 2-4.

In the synchronous case, there is no time difference between each user signal and the channel coefficients are the same for all users. Also, the phase shift caused by the carrier signal generator is equivalent for all users since only one oscillator is employed to generate all signals. Thus, in order to analyze the synchronous case, a few parameters in Equation (2-15) should be modified as follows:

$$\tau_k = 0,$$

$\alpha_{k,l} \to \alpha_l$,

$\tau_{k,l} \to \tau_l$,

$\phi_k \to \phi$ (constant),

$\varphi_{k,l} \to \varphi_l$,

$\theta_{k,l} \to \theta_l = \phi + \varphi_l$,

for $k = 1, 2, \cdots, K$. With these modified parameters, the received signal for the synchronous case can be expressed as

$$\tilde{r}_s(t) = \mathrm{Re}\{r_s(t)e^{j\omega_c t}\}, \tag{2-38}$$

where the complex baseband expression $r_s(t)$ is equal to

$$\begin{aligned} r_s(t) = n(t) + \frac{1}{2}\sum_{k=1}^{K}\sum_{l=1}^{L}\alpha_l\{&\sqrt{p_k}b_{k,I}(t-\tau_l)a_k(t-\tau_l) \\ &+ j\sqrt{p_k}b_{k,Q}(t-\tau_l)a_k(t-\tau_l)\}e^{j\theta_l}. \end{aligned} \tag{2-39}$$

For the sake of simplicity, the in-phase term and the quadrature term in Equation (2-39) are represented as follows:

$$In_{k,l}^{(s)} = \sqrt{p_k}b_{k,I}(t-\tau_l)a_k(t-\tau_l), \tag{2-40}$$

$$Qu_{k,l}^{(s)} = \sqrt{p_k}b_{k,Q}(t-\tau_l)a_k(t-\tau_l). \tag{2-41}$$

Analogously to Equation (2-19), Equation (2-38) can be written as

$$\tilde{r}_s(t) = \tilde{n}(t) + \frac{1}{2}\sum_{k=1}^{K}\sum_{l=1}^{L}\alpha_l\{In_{k,l}^{(s)}\cos(\omega_c t + \theta_l) - Qu_{k,l}^{(s)}\sin(\omega_c t + \theta_l)\}. \tag{2-42}$$

Similarly, the decision statistics are analogous with $z'_{k,m,\mathrm{Re}}$ and $z'_{k,m,\mathrm{Im}}$ which may be represented as

$$z'^{(s)}_{k,m,\mathrm{Re}} = \int_{\tau_{l^{(m)}}}^{\tau_{l^{(m)}}+T_s} [\{\tilde{n}(t) + \frac{1}{2}\sum_{k'=1}^{K}\sum_{l=1}^{L}\alpha_l (In^{(s)}_{k',l}\cos(\omega_c t + \theta_l) - Qu^{(s)}_{k',l}\sin(\omega_c t + \theta_l))\}\{\cos(\omega_c t + \theta_{l^{(m)}})a_k(t-\tau_{l^{(m)}})\}]dt \tag{2-43}$$

$$= \xi_I + A^{(s)}_I + \sum_{\substack{l=1 \\ l\neq l^{(m)}}}^{L} I^{(s)}_{k,l,\mathrm{Re}} + \sum_{\substack{k'=1 \\ k'\neq k}}^{K}\sum_{l=1}^{L} I^{(s)}_{k',l,\mathrm{Re}}\ , \tag{2-44}$$

and

$$z'^{(s)}_{k,m,\mathrm{Im}} = \int_{\tau_{l^{(m)}}}^{\tau_{l^{(m)}}+T_s} [\{\tilde{n}(t) + \frac{1}{2}\sum_{k'=1}^{K}\sum_{l=1}^{L}\alpha_l (In^{(s)}_{k',l}\cos(\omega_c t + \theta_l) - Qu^{(s)}_{k',l}\sin(\omega_c t + \theta_l))\}\{-\sin(\omega_c t + \theta_{l^{(m)}})a_k(t-\tau_{l^{(m)}})\}]dt \tag{2-45}$$

$$= \xi_Q + A^{(s)}_Q + \sum_{\substack{l=1 \\ l\neq l^{(m)}}}^{L} I^{(s)}_{k,l,\mathrm{Im}} + \sum_{\substack{k'=1 \\ k'\neq k}}^{K}\sum_{l=1}^{L} I^{(s)}_{k',l,\mathrm{Im}}\ , \tag{2-46}$$

where ξ_I and ξ_Q represent the contribution of the Gaussian noise $\tilde{n}(t)$ in the in-phase component and the quadrature component, respectively. The desired signal components $A^{(s)}_I$ and $A^{(s)}_Q$, and the interference components $I^{(s)}_{k,l,\mathrm{Re}}$, $I^{(s)}_{k,l,\mathrm{Im}}$, $I^{(s)}_{k',l,\mathrm{Re}}$ and $I^{(s)}_{k',l,\mathrm{Im}}$ can be derived analogously to A_I, A_Q, $I_{k,l,\mathrm{Re}}$, $I_{k,l,\mathrm{Im}}$, $I_{k',l,\mathrm{Re}}$ and $I_{k',l,\mathrm{Im}}$ in the following:

$$A^{(s)}_I = \frac{1}{4}\sqrt{p_k}\alpha_{l^{(m)}} b^i_{k,I} T_s\ , \tag{2-47}$$

$$A^{(s)}_Q = \frac{1}{4}\sqrt{p_k}\alpha_{l^{(m)}} b^i_{k,Q} T_s\ , \tag{2-48}$$

$$I^{(s)}_{k,l,\mathrm{Re}} = \frac{1}{4}\sqrt{p_k}\alpha_l [\{\cos(\theta_l - \theta_{l^{(m)}})\times \int_{\tau_{l^{(m)}}}^{\tau_{l^{(m)}}+T_s} b_{k,I}(t-\tau_l)a_k(t-\tau_l)\cdot a_k(t-\tau_{l^{(m)}})dt\} - \{\sin(\theta_l - \theta_{l^{(m)}})\times \int_{\tau_{l^{(m)}}}^{\tau_{l^{(m)}}+T_s} b_{k,Q}(t-\tau_l)\cdot a_k(t-\tau_l)a_k(t-\tau_{l^{(m)}})dt\}], \tag{2-49}$$

$$I_{k,l,\mathrm{Im}}^{(s)} = \frac{1}{4}\sqrt{p_k}\alpha_l[\{(-1)\sin(\theta_l - \theta_{l^{(m)}}) \times \int_{\tau_{l^{(m)}}}^{\tau_{l^{(m)}}+T_s} b_{k,I}(t-\tau_l)a_k(t-\tau_l)\cdot a_k(t-\tau_{l^{(m)}})dt\}$$
$$+\{\cos(\theta_l - \theta_{l^{(m)}}) \times \int_{\tau_{l^{(m)}}}^{\tau_{l^{(m)}}+T_s} b_{k,Q}(t-\tau_l)\cdot a_k(t-\tau_l)a_k(t-\tau_{l^{(m)}})dt\}], \quad (2\text{-}50)$$

$$I_{k',l,\mathrm{Re}}^{(s)} = \frac{1}{4}\sqrt{p_{k'}}\alpha_l[\{\cos(\theta_l - \theta_{l^{(m)}}) \times \int_{\tau_{l^{(m)}}}^{\tau_{l^{(m)}}+T_s} b_{k',I}(t-\tau_l)a_{k'}(t-\tau_l)\cdot a_k(t-\tau_{l^{(m)}})dt\}$$
$$-\{\sin(\theta_l - \theta_{l^{(m)}}) \times \int_{\tau_{l^{(m)}}}^{\tau_{l^{(m)}}+T_s} b_{k',Q}(t-\tau_l)\cdot a_{k'}(t-\tau_l)a_k(t-\tau_{l^{(m)}})dt\}], \quad (2\text{-}51)$$

$$I_{k',l,\mathrm{Im}}^{(s)} = \frac{1}{4}\sqrt{p_{k'}}\alpha_l[\{(-1)\sin(\theta_l - \theta_{l^{(m)}}) \times \int_{\tau_{l^{(m)}}}^{\tau_{l^{(m)}}+T_s} b_{k',I}(t-\tau_l)a_{k'}(t-\tau_l)\cdot a_k(t-\tau_{l^{(m)}})dt\}$$
$$+\{\cos(\theta_l - \theta_{l^{(m)}}) \times \int_{\tau_{l^{(m)}}}^{\tau_{l^{(m)}}+T_s} b_{k',Q}(t-\tau_l)\cdot a_{k'}(t-\tau_l)a_k(t-\tau_{l^{(m)}})dt\}]. \quad (2\text{-}52)$$

Therefore, the final decision statistic can be expressed as

$$z_{k,\mathrm{Re}}^{(s)} = \sum_{m=1}^{M} \alpha_m z_{k,m,\mathrm{Re}}^{\prime(s)} \quad (2\text{-}53)$$

for the in-phase part, and

$$z_{k,\mathrm{Im}}^{(s)} = \sum_{m=1}^{M} \alpha_m z_{k,m,\mathrm{Im}}^{\prime(s)} \quad (2\text{-}54)$$

for the quadrature part, where the weight α_m is the amplitude of the complex channel coefficient.

2.4. Chapter Summary

CDMA based on DS/SS (Direct Sequence / Spread Spectrum) communications forms the basis of third generation personal communications systems. The popular air interface standards WCDMA [14] and cdma 2000 [14] both feature elaborate CDMA

waveforms. In this chapter we have laid out a mathematical abstraction of a DS/SS CDMA waveform which captures several key features of interest. We have assumed QPSK modulation, and rectangular pulse shaping. We have allowed for arbitrary numbers of users, numbers of multipath and data rates. We have presented complete model of the transmitter, channel, and receiver for both the uplink and downlink.

Chapter 3. Simulation Approach

In the previous we laid out a mathematical model for CDMA communications. In this chapter we present the implementation details of a simulation based on that mathematical model.

3.1. Generation of AWGN

When transmitted signals arrive at a receiver, thermal noise is added to transmitted signals at the front end of the receiver. We model the thermal noise as the additive white Gaussian noise (AWGN). This section explains how the noise term of the received signal representation is modeled in the simulation. $s_k(t)$ in Equation (2-3) is the complex baseband representation of the transmitted signal and the corresponding signal constellations is illustrated in Figure 3-1.

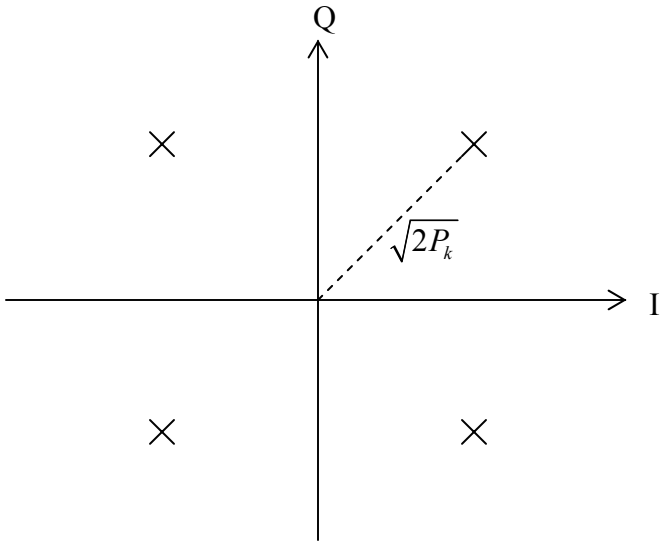

Figure 3-1. QPSK signal constellations

P_k is the power of one bit and $\sqrt{2P_k}$ is the magnitude of one symbol since the QPSK modulation scheme is used. They can be expressed as

$$P_k = \frac{E_b \cdot r}{SF \cdot m} \tag{3-1}$$

$$A = \sqrt{2P_k} \tag{3-2}$$

where E_b : energy per data bit;

r : rate of error control code;

SF : spreading factor;

m : samples per symbol,

and A is magnitude of the modulation symbol. In simulation, E_b is assumed to be one, and noise is scaled to produce the desired E_b/N_0. The noise samples to be added are written as

$$n = x + jy$$

where x is in-phase part and y is quadrature part of noise sample. x and y are Gaussian random variables with the same variance which is

$$\begin{aligned}\sigma_x^2 = \sigma_y^2 &= \frac{Expectation\ of\ noise\ power}{2} = \frac{A^2}{2(E_s/N_0)} = \frac{A^2}{2(2E_b/N_0)} \\ &= \frac{2P_k}{4(E_b/N_0)} = \frac{P_k}{2(E_b/N_0)}\end{aligned} \tag{3-3}$$

where E_s is energy per QPSK modulated symbol.

3.2. Channel Model

For simulation of frequency selective and slow fading channels, the modified Jakes' model in [13] is used. This modified channel model generates time-uncorrelated Rayleigh fading waveforms while the Jakes' deterministic fading model is for simulating time-correlated waveforms [13].

"The advantage of the modified Jakes' model over other forms of fading simulator lies in its greatly reduced executing time and capability for simultaneous generation of multiple uncorrelated fading signals [13]." The fading waveform for the l^{th} path is represented by

$$\alpha_{k,l} e^{j\psi_{k,l}} = X_{c,l}(t) + jX_{s,l}(t), \tag{3-4}$$

$$X_{c,l}(t) = 2\sum_{n=1}^{L_0} \cos\theta_{n,l} \cos\left(\omega_n t + \frac{\pi l}{2}\right), \tag{3-5}$$

$$X_{s,l}(t) = 2\sum_{n=1}^{L_0} \sin\theta_{n,l} \cos\left(\omega_n t + \frac{\pi l}{2}\right), \tag{3-6}$$

where L_0 : Number of oscillators;

$N = 4(L_0 + 1)$;

v : Vehicle speed;

f_c : Carrier frequency;

c : Speed of light;

Maximum Doppler shift $\omega_M = \dfrac{2\pi f_c v}{c}$;

Doppler shift $\omega_n = \omega_M \cos\dfrac{2\pi(n-0.5)}{N}$,

and $\theta_{n,l} = \dfrac{\pi nl}{L_0}$, $(j = 1,\ 2,\ \cdots,\ L_0 - 1)$.

In Equation (3-4), the random variables are deterministic with time and path. This random process is ergodic and the fading waveforms are uncorrelated to each other. Therefore, one Rayleigh distributed and the other uniform distributed random variable can be obtained from the magnitude and phase of Equation (3-4).

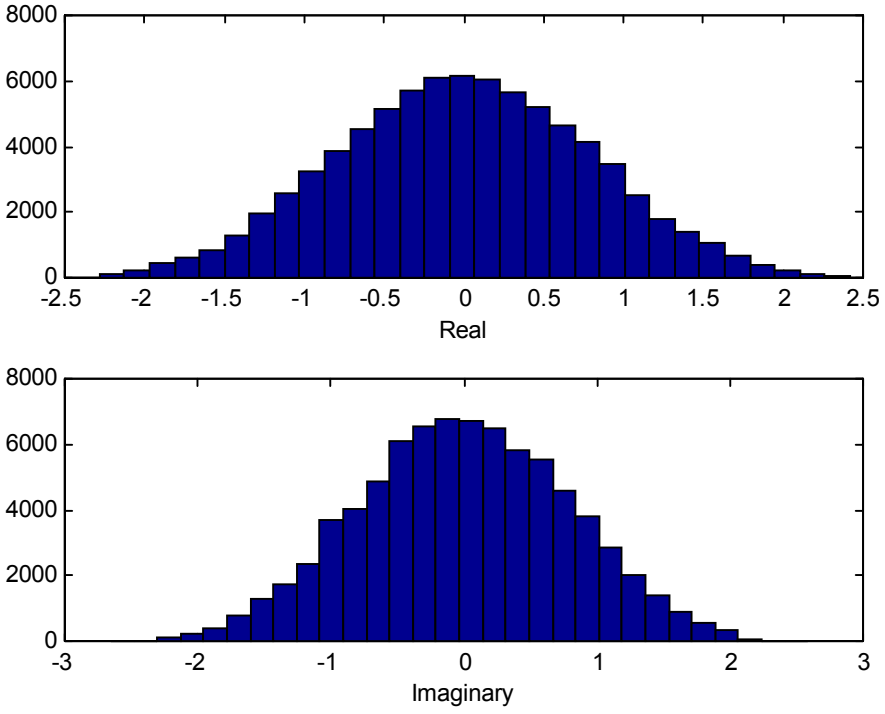

(a) Real and imaginary value distribution

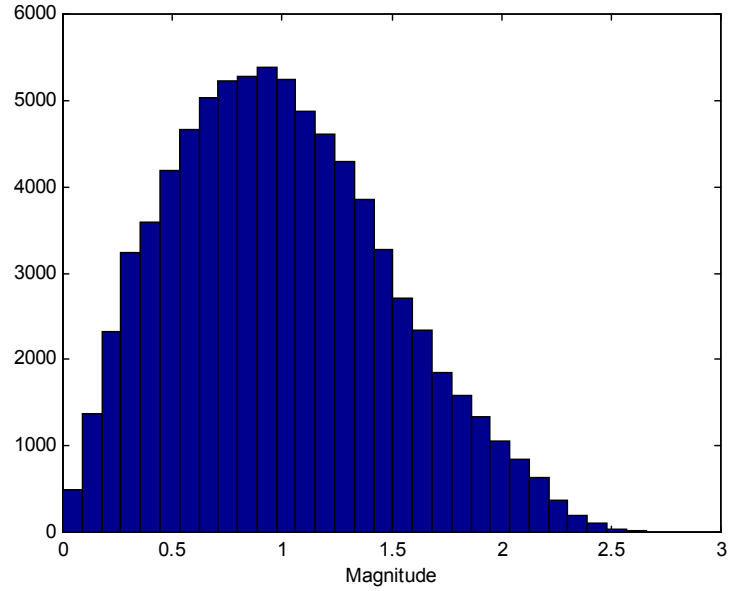

(b) Magnitude distribution

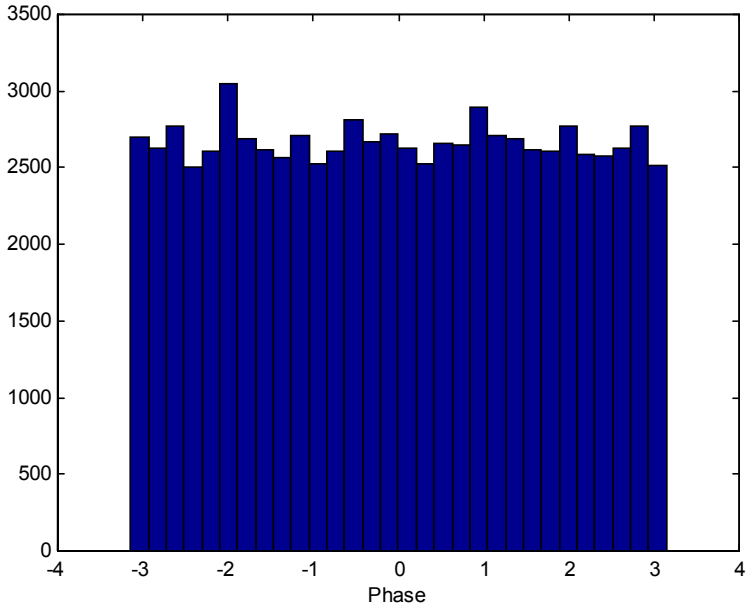

(c) Phase distribution

Figure 3-2. Histograms of Jakes' modified model waveform

Figure 3-2 shows the distributions of 80000 samples of a waveform from the modified Jakes' model. The Gaussian distributions of $X_{c,l}(t)$ and $X_{s,l}(t)$ in Equation (3-4) are presented in Figure 3-2 (a). The Rayleigh distribution of $\alpha_{k,l}$ is shown in Figure 3-2 (b). The uniform distribution of $e^{j\psi_{k,l}}$ is shown in Figure 3-2 (c).

For the simulation, the values of channel parameters are set arbitrarily, according to Table 3-1. These parameters are intended to model on urban microcell environment, which is among the most challenging environments from a capacity perspective.

Table 3-1. Power delay profile

Path	Delay [μ s]	Attenuation [dB]
1	0	0
2	0.68	-3
3	1.7	-6

The choice of the delay and attenuation parameters is according to a power delay profile of a specific channel environment. Indoor or outdoor, urban or rural, and macrocell or microcell channel environment each leads to a different power delay profile. Since the number of multipath is three, the number of the fingers of the Rake receiver is less or equal to three. For simulations in frequency selective fading channel environment, chip duration should be less than delay.

3.3. Orthogonal Variable Spreading Factor (OVSF) codes

In WCDMA system, the Hadamard codes called OVSF codes are used for spreading message signals. In general, the OVSF code of length 2^{n+1} is generated through the procedure described in Figure 3-3 [10].

$$C_{1,0} = 1$$

$$\begin{bmatrix} C_{2,0} \\ C_{2,1} \end{bmatrix} = \begin{bmatrix} C_{1,0} & C_{1,0} \\ C_{1,0} & -C_{1,0} \end{bmatrix} = \begin{bmatrix} 1 & 1 \\ 1 & -1 \end{bmatrix}$$

...

$$\begin{bmatrix} C_{2^{n+1},0} \\ C_{2^{n+1},1} \\ C_{2^{n+1},2} \\ C_{2^{n+1},3} \\ \vdots \\ C_{2^{n+1},2^{n+1}-2} \\ C_{2^{n+1},2^{n+1}-1} \end{bmatrix} = \begin{bmatrix} C_{2^n,0} & C_{2^n,0} \\ C_{2^n,0} & -C_{2^n,0} \\ C_{2^n,1} & C_{2^n,1} \\ C_{2^n,1} & -C_{2^n,1} \\ \vdots & \vdots \\ C_{2^n,2^n-1} & C_{2^n,2^n-1} \\ C_{2^n,2^n-1} & -C_{2^n,2^n-1} \end{bmatrix}$$

Figure 3-3. Generating procedure for OVSF code

The notation $C_{SF,k}$ means the k^{th} code with the spreading factor SF. The spreading factor should be a power of 2, and for a given SF, there are SF orthogonal codes which differ from each other in exactly $\frac{SF}{2}$ positions. Also, orthogonality is preserved even between some two codes with different SF s. However, if one code is one of the mother codes of the other one, they are not orthogonal to each other and can not be

used for spreading codes simultaneously. Therefore, the spreading factor of one user restricts the number of available codes for the other users.

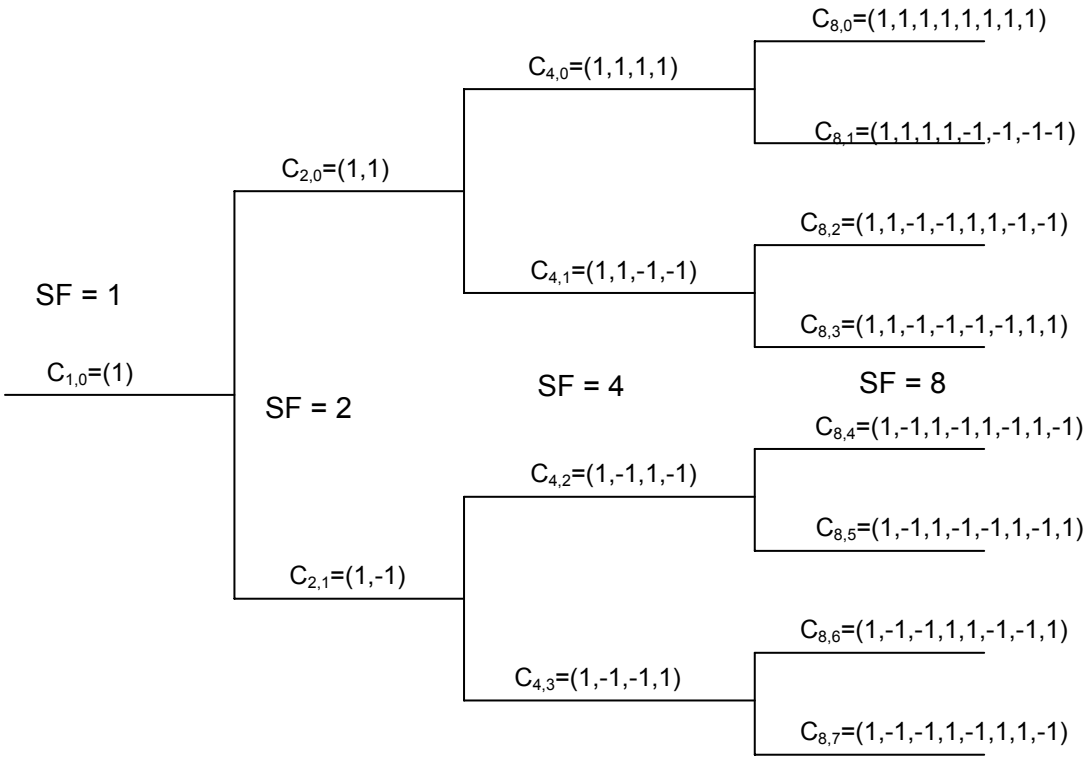

Figure 3-4. OVSF codes

In Figure 3-4, $C_{4,2}$ is the mother code of $C_{8,4}$ and $C_{8,5}$. The auto-correlation of the OVSF codes is quite poor even though they are orthogonal to each other. In Figure 3-5, auto and cross-correlation properties of OVSF codes are presented.

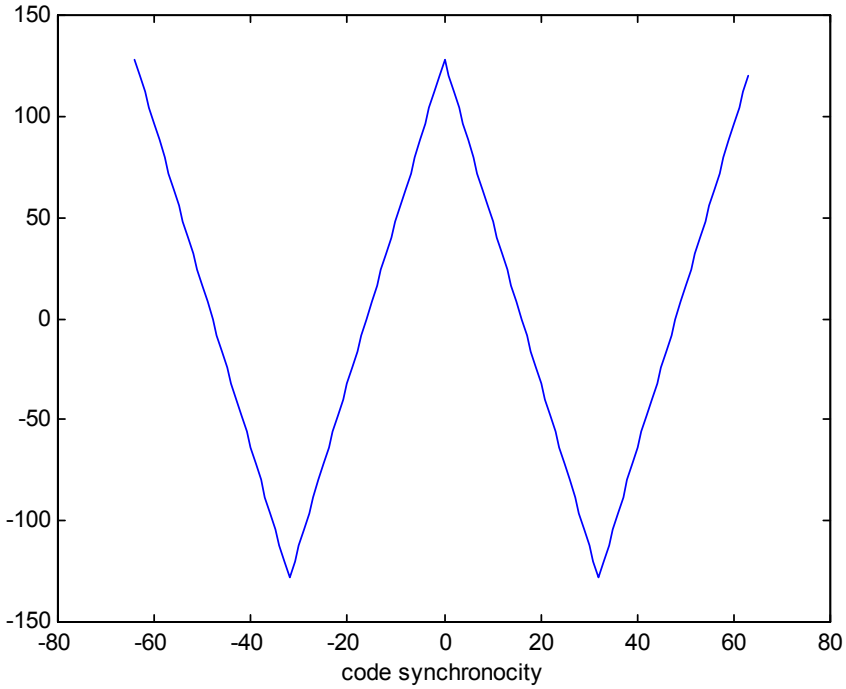

(a)

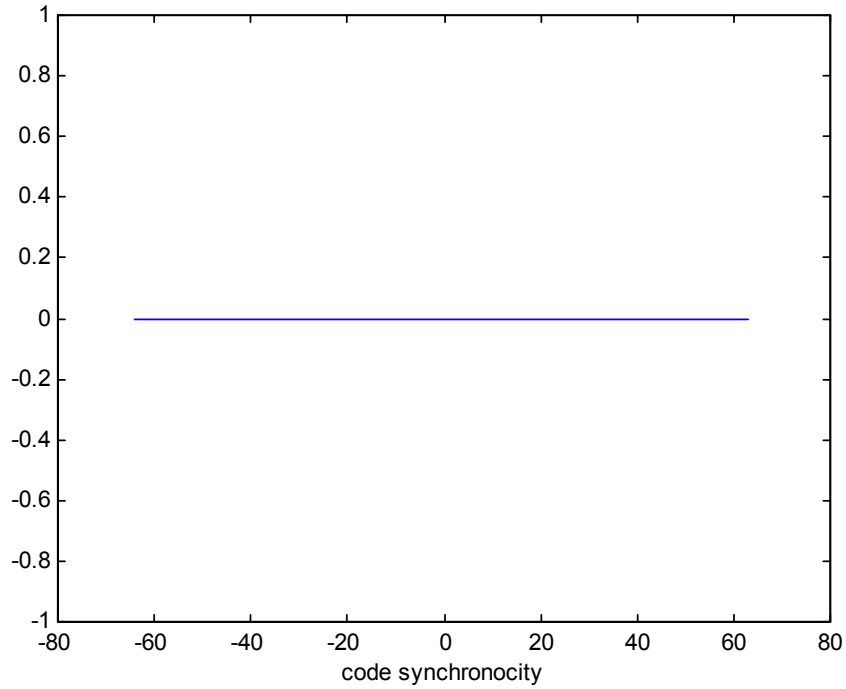

(b)

Figure 3-5. Correlations of OVSF (*SF* =128)

(a) Auto-correlation, (b) Cross-correlation

3.4. Simulation Assumptions

Some assumption should be made for simulation of the CDMA system described in the previous chapter. First, the simulation is based on a baseband signal. Thus, symbols, noise, and multipath fading are represented in complex baseband form instead of multiplying by a high-frequency sinusoidal carrier. For an analytical description of the simulation condition, it is assumed that the carrier frequency is 2 GHz and the chip rate is 3.84 Mcps. This assumption is in accordance with the WCDMA standards. However, the simulation results cannot be compared with the performance of a commercial WCDMA system since the simulation condition does not satisfy with the other WCDMA standards.

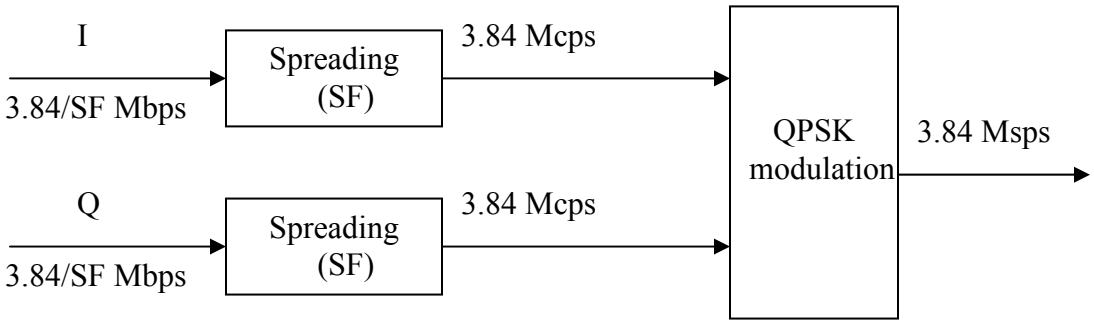

Figure 3-6. Data rate

(bps : bits per second, cps : chips per second, sps : symbols per second)

Short spreading codes are used for simulation. In Figure 3-6, SF denotes the length of spreading code and is the abbreviation for spreading factor. The data rate is variable according to the value of SF . Therefore, the general expression for the data rate is $(2\times 3.84)/SF$ Mbps. The first null bandwidth is 3.84 MHz since the rectangular pulse shaping is used in this simulation. The WCDMA standard employs raised cosine pulse

shaping with a roll-off factor of 0.22. While pulse shape plays a significant role in determining the spectral characteristics of the signal, and may play a factor in performance if timing offset is an issue, it dose not heavily influence the performance of the system in multipath and multiple access interference. In order to reduce simulation complexity, we use rectangular pulse shapes in this thesis. The values of the carrier frequency and chip duration are required to generating the Rayleigh fading channel waveforms using the modified Jakes' model.

3.5. Gaussian Approximation for QPSK

In this section, the Gaussian approximation for the performance of DS-CDMA system using QPSK modulation scheme is derived in the AWGN channel environment. The well-known Gaussian approximation for BPSK is extended to the case of QPSK.

Assuming the phase of carrier signal ϕ_1 and the delay τ_1 for 1^{st} user are equal to zero, the transmitted signal of 1^{st} user can be expressed as

$$\tilde{s}_1(t) = \mathrm{Re}\left\{\left(\sqrt{p_1}b_{1,I}(t)a_1(t) + j\sqrt{p_1}b_{1,Q}(t)a_1(t)\right)e^{j\omega_c t}\right\}. \tag{3-7}$$

Including the other $K-1$ concurrent users' signals, the received signal can be represented by

$$\tilde{r}(t) = \tilde{s}_1(t) + \tilde{n}(t) + \sum_{k=2}^{K}\tilde{s}_k(t-\tau_k). \tag{3-8}$$

At the output of the correlators, the decision statistics of in-phase and quadrature component are expressed as

$$z_{1,\mathrm{Re}} = \int_0^{T_s}\tilde{r}(t)a_1(t)\cos(\omega_c t)\,dt = A_{1,I} + \xi_I + \sum_{k=2}^{K} I_{k,\mathrm{Re}} \tag{3-9}$$

and

$$z_{1,\mathrm{Im}} = \int_0^{T_s} \tilde{r}(t) a_1(t) \left\{ -\sin\left(\omega_c t\right) \right\} dt = A_{1,Q} + \xi_Q + \sum_{k=2}^{K} I_{k,\mathrm{Im}} \ . \tag{3-10}$$

$A_{1,I}$ and $A_{1,Q}$ in Equation (3-9) and (3-10) represent the desired signal terms as follows. Assuming $f_c T_s \gg 1$ and $b_{1,I} = b_{1,Q} = 1$, $A_{1,I}$ is

$$\begin{aligned}
A_{1,I} &= \int_0^{T_s} \tilde{s}_1(t) a_1(t) \cos(\omega_c t) dt \\
&= \int_0^{T_s} \left\{ \sqrt{p_1} b_{1,I}(t) a_1(t) \cos(\omega_c t) - \sqrt{p_1} b_{1,Q}(t) a_1(t) \sin(\omega_c t) \right\} a_1(t) \cos(\omega_c t) dt \\
&= \int_0^{T_s} \left\{ \sqrt{p_1} b_{1,I}(t) \cos^2(\omega_c t) - \sqrt{p_1} b_{1,Q}(t) \sin(\omega_c t) \cos(\omega_c t) \right\} dt \\
&= \frac{\sqrt{p_1}}{2} \int_0^{T_s} b_{1,I}(t) dt \\
&= \frac{\sqrt{p_1}}{2} T_s \ ,
\end{aligned} \tag{3-11}$$

and $A_{1,Q}$ is

$$\begin{aligned}
A_{1,Q} &= \int_0^{T_s} \tilde{s}_1(t) a_1(t) \left\{ -\sin(\omega_c t) \right\} dt \\
&= \int_0^{T_s} \left\{ \sqrt{p_1} b_{1,I}(t) a_1(t) \cos(\omega_c t) - \sqrt{p_1} b_{1,Q}(t) a_1(t) \sin(\omega_c t) \right\} a_1(t) \left\{ -\sin(\omega_c t) \right\} dt \\
&= \int_0^{T_s} \left\{ -\sqrt{p_1} b_{1,I}(t) \cos(\omega_c t) \sin(\omega_c t) + \sqrt{p_1} b_{1,Q}(t) \sin^2(\omega_c t) \right\} dt \\
&= \frac{\sqrt{p_1}}{2} \int_0^{T_s} b_{1,Q}(t) dt \\
&= \frac{\sqrt{p_1}}{2} T_s \ .
\end{aligned} \tag{3-12}$$

ξ_I and ξ_Q are the contribution of the Gaussian noise $\tilde{n}(t)$, and represented by

$$\xi_I = \int_0^{T_s} \tilde{n}(t) a_1(t) \cos(\omega_c t) dt \,, \tag{3-13}$$

and

$$\xi_Q = \int_0^{T_s} \tilde{n}(t) a_1(t) \{-\sin(\omega_c t)\} dt \,. \tag{3-14}$$

The mean of ξ_I is

$$E[\xi_I] = E\left[\int_0^{T_s} \tilde{n}(t) a_1(t) \cos(\omega_c t) dt\right] = \int_0^{T_s} E[\tilde{n}(t)] a_1(t) \cos(\omega_c t) dt = 0 \,, \tag{3-15}$$

and the mean of ξ_Q is

$$E[\xi_Q] = E\left[\int_0^{T_s} \tilde{n}(t) a_1(t) \{-\sin(\omega_c t)\} dt\right] = \int_0^{T_s} E[\tilde{n}(t)] a_1(t) \{-\sin(\omega_c t)\} dt = 0 \,. \tag{3-16}$$

The variance of ξ_I is

$$\begin{aligned} E[\xi_I^2] &= E\left[\int_0^{T_s} \tilde{n}(t) a_1(t) \cos(\omega_c t) dt \int_0^{T_s} \tilde{n}(s) a_1(s) \cos(\omega_c s) ds\right] \\ &= \int_0^{T_s}\int_0^{T_s} E[\tilde{n}(t)\tilde{n}(s)] a_1(t) \cos(\omega_c t) a_1(s) \cos(\omega_c s) dt ds \\ &= \int_0^{T_s}\int_0^{T_s} \frac{N_0}{2} \delta(t-s) a_1(t) \cos(\omega_c t) a_1(s) \cos(\omega_c s) dt ds \\ &= \int_0^{T_s} \frac{N_0}{2} a_1^2(t) \cos^2(\omega_c t) dt \\ &= \frac{N_0}{4} T_s \,, \end{aligned} \tag{3-17}$$

and the variance of ξ_Q is

$$
\begin{aligned}
E\left[\xi_Q^2\right] &= E\left[\int_0^{T_s} \tilde{n}(t)a_1(t)\left\{-\sin(\omega_c t)\right\}dt \int_0^{T_s} \tilde{n}(s)a_1(s)\left\{-\sin(\omega_c s)\right\}ds\right] \\
&= \int_0^{T_s}\int_0^{T_s} E\left[\tilde{n}(t)\tilde{n}(s)\right]a_1(t)\sin(\omega_c t)a_1(s)\sin(\omega_c s)dtds \\
&= \int_0^{T_s}\int_0^{T_s} \frac{N_0}{2}\delta(t-s)a_1(t)\sin(\omega_c t)a_1(s)\sin(\omega_c s)dtds \\
&= \int_0^{T_s} \frac{N_0}{2}a_1^2(t)\sin^2(\omega_c t)dt \\
&= \frac{N_0}{4}T_s \ . \qquad (3-18)
\end{aligned}
$$

$I_{k,\mathrm{Re}}$ and $I_{k,\mathrm{Im}}$ are the interference caused by k^{th} user. $I_{k,\mathrm{Re}}$ can be expressed as

$$
\begin{aligned}
I_{k,\mathrm{Re}} &= \int_0^{T_s} \tilde{s}(t-\tau_k)a_1(t)\cos(\omega_c t)dt \\
&= \int_0^{T_s} \left\{\sqrt{p_k}b_{k,I}(t-\tau_k)a_k(t-\tau_k)\cos(\omega_c t+\theta_k) - \sqrt{p_k}b_{k,Q}(t-\tau_k)a_k(t-\tau_k)\sin(\omega_c t+\theta_k)\right\} \\
&\quad \cdot a_1(t)\cos(\omega_c t)dt \\
&= \frac{\sqrt{p_k}}{2}\cos(\theta_k)\int_0^{T_s} b_{k,I}(t-\tau_k)a_k(t-\tau_k)a_1(t)dt \\
&\quad -\frac{\sqrt{p_k}}{2}\sin(\theta_k)\int_0^{T_s} b_{k,Q}(t-\tau_k)a_k(t-\tau_k)a_1(t)dt, \qquad (3-19)
\end{aligned}
$$

and $I_{k,\mathrm{Im}}$ can be expressed as

$$
\begin{aligned}
I_{k,\mathrm{Im}} &= \int_0^{T_s} \tilde{s}(t-\tau_k)a_1(t)\left\{-\sin(\omega_c t)\right\}dt \\
&= \int_0^{T_s} \left\{\sqrt{p_k}b_{k,I}(t-\tau_k)a_k(t-\tau_k)\cos(\omega_c t+\theta_k) - \sqrt{p_k}b_{k,Q}(t-\tau_k)a_k(t-\tau_k)\sin(\omega_c t+\theta_k)\right\} \\
&\quad \cdot a_1(t)\left\{-\sin(\omega_c t)\right\}dt \\
&= -\frac{\sqrt{p_k}}{2}\sin(\theta_k)\int_0^{T_s} b_{k,I}(t-\tau_k)a_k(t-\tau_k)a_1(t)dt \\
&\quad +\frac{\sqrt{p_k}}{2}\cos(\theta_k)\int_0^{T_s} b_{k,Q}(t-\tau_k)a_k(t-\tau_k)a_1(t)dt, \qquad (3-20)
\end{aligned}
$$

where the random phase θ_k is uniformly distributed on the range between 0 and 2π. The first and second term of $I_{k,\mathrm{Re}}$ and $I_{k,\mathrm{Im}}$ has zero mean and the same variance as the interference of DS-CDMA using a BPSK modulation scheme. Therefore, the average power of interference for QPSK is double that of BPSK.

The well-known bit error probability of BPSK is expressed as

$$P_{b,BPSK} = Q\left(\sqrt{\frac{2E_b}{N_0 + p_J/W}}\right) = Q\left(1\Big/\sqrt{\frac{N_0}{2E_b} + \frac{p_J}{2E_bW}}\right), \tag{3-21}$$

where p_J is the average power of interference and W is the bandwidth of spread spectrum signal [17]. E_b can be expressed as

$$E_b = T_b p_s = \frac{p_s}{R_b}, \tag{3-22}$$

where T_b is the time period of information bits, p_s is the average power of desired signal, and R_b is information data rate. Substituting with Equation (3-22), Equation (3-21) can be rewritten by

$$P_{b,BPSK} = Q\left(1\Big/\sqrt{\frac{N_0}{2E_b} + \frac{p_J}{2p_sN}}\right), \tag{3-23}$$

where N is the processing gain and equal to W/R_b. To calculate the error probability of QPSK, two parameters in Equation (3-23) should be changed. One is p_J substituted by $2\times p_J$ since the interference level of QPSK increases by a factor of 2. The other is due to the reduction of information data bandwidth. For QPSK, R_b decreases by a factor of 2. As a result, the Gaussian approximation of QPSK is the same as that of BPSK, and expressed as

$$P_{b,QPSK} = Q\left(1\Big/\sqrt{\frac{N_0}{2E_b} + \frac{2 \cdot p_J}{2 \cdot 2 p_s N}}\right) = P_{b,BPSK}\,, \tag{3-24}$$

where $p_J = \sum_{\substack{k=1 \\ k \neq s}}^{K} p_k$.

3.6. Simulation Results

In this section, computer simulation results are shown to verify how the channel environment and various parameters affect the performance of a CDMA system. The computer programming for simulation is based on the previous mathematical description and assumptions. All simulation results are for the performance on the uplink from mobile handsets to a base station.

No multipath fading	# of fingers	SF
	1	16

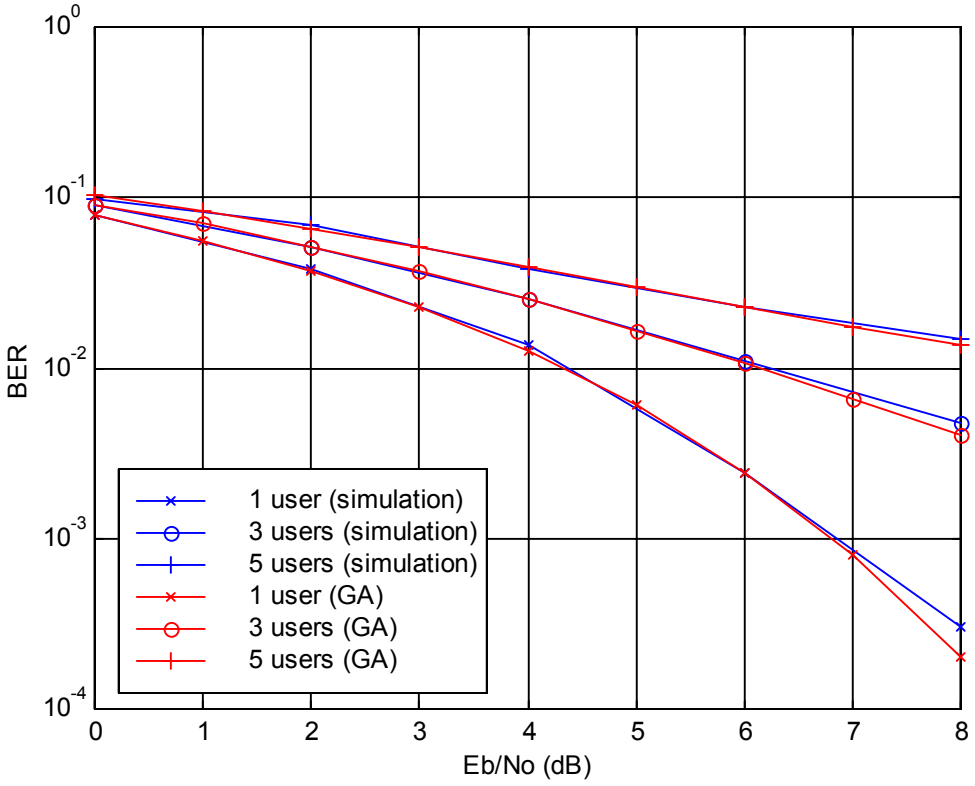

Figure 3-7 (a): Analytical and Simulated BER vs. E_b/N_0 of a DS-QPSK system (SF=16).

No multipath fading	# of fingers	SF
	1	8

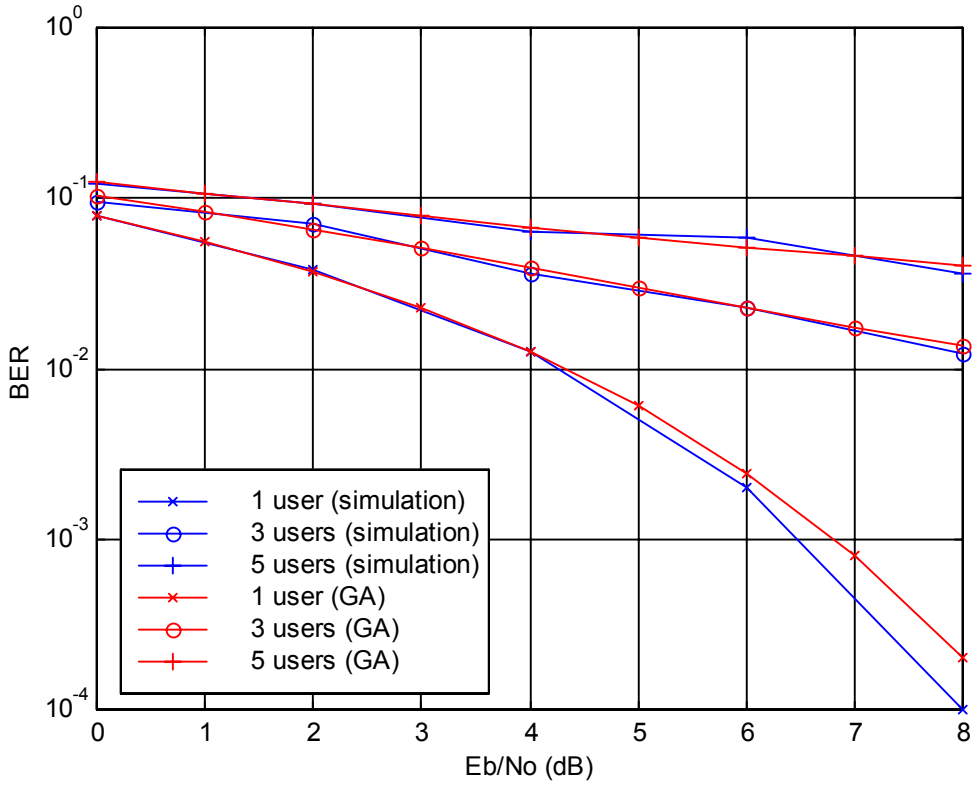

Figure 3-7 (b): Analytical and Simulated BER for a DS-QPSK system (SF=8).

Figure 3-7 compares the performance in three cases of one, three and five users in an AWGN channel. There is no multipath. The spreading factor is 16 in Figure 3-7(a), and 8 in Figure 3-7(b). The Gaussian approximation (GA) provides some validation of the simulation results. Comparing between Figures 3-7 (a) and (b), it is apparent that as the SF decreases, the mean interference between users increases, resulting in corresponding degradation in BER performance.

No multipath fading	# of fingers	SF
	1	16

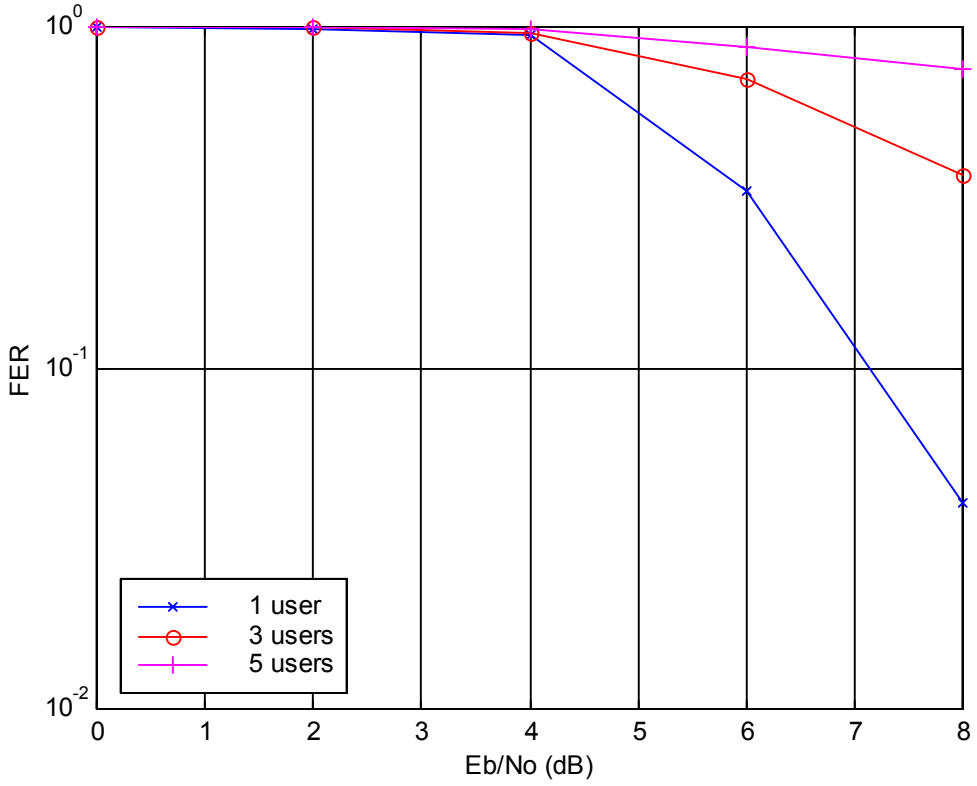

(a) SF=16

No multipath fading	# of fingers	SF
	1	8

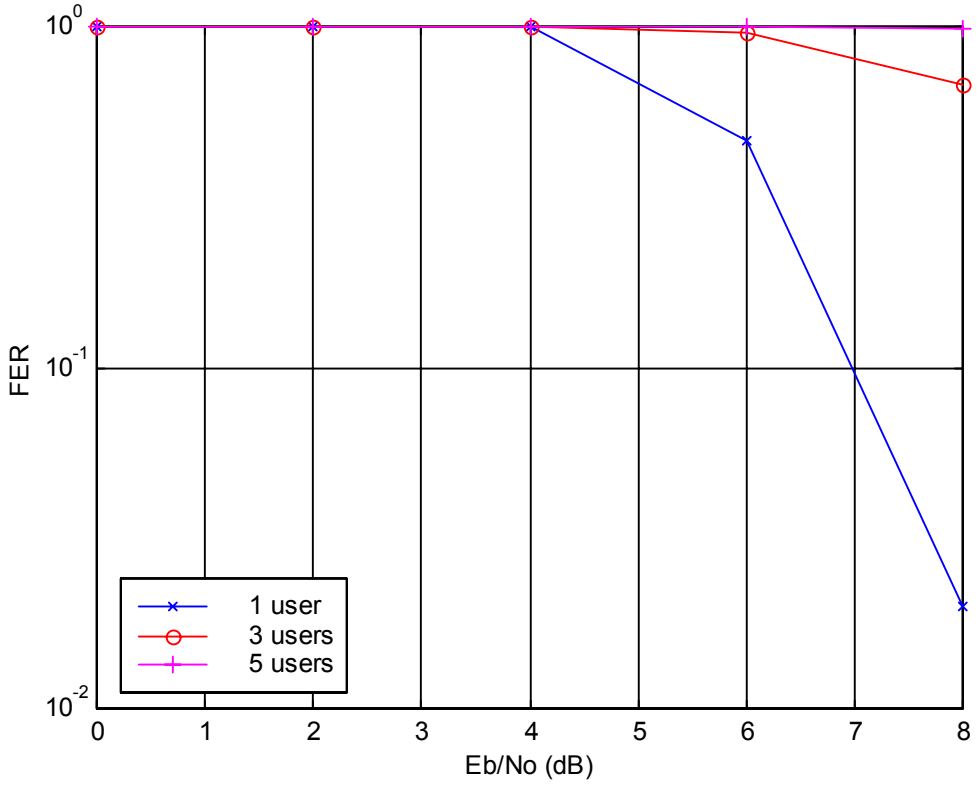

(b) SF=8

Figure 3-8. Different number of users in AWGN channel (FER)

In Figure 3-8, the simulation result in Figure 3-7 shows the Frame Error Rate (FER) for the situation corresponding to Figure 3-7. One frame consists of 2560 chips, so 160 information bits are transmitted in each frame since the spreading factor is 16. In the case of three users, more erroneous frames are expected at the receiver due to the increase of interference.

Only one path	# of fingers	# of users	SF	Speed of user
	1	3	16	100 km/h

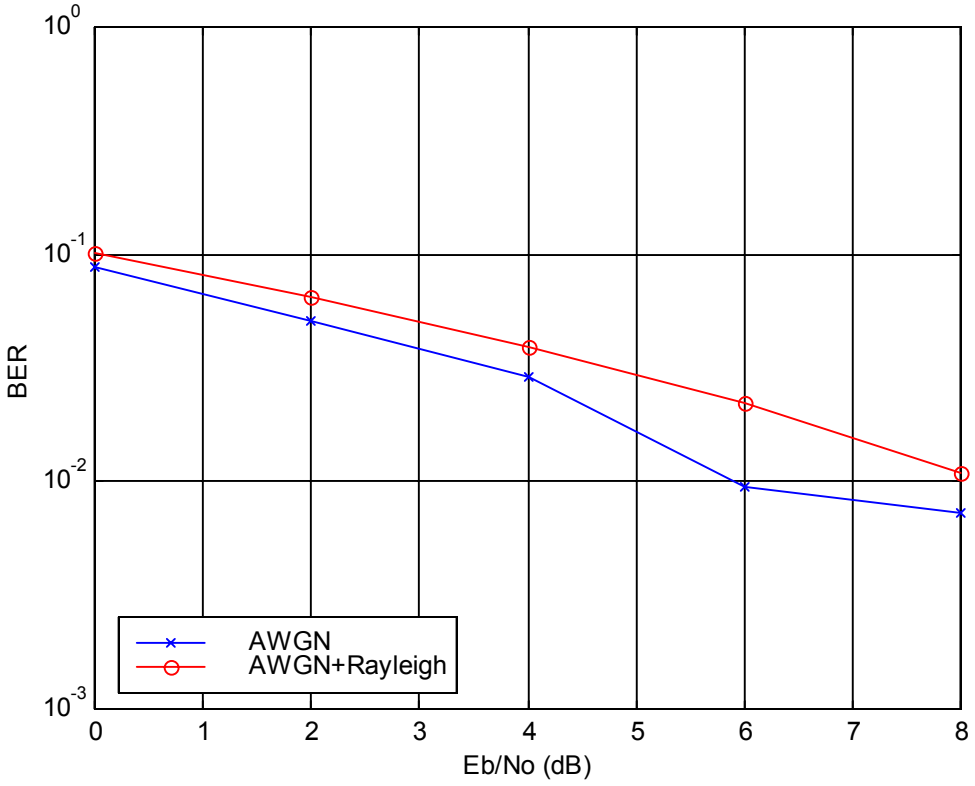

Figure 3-9. Effect of Rayleigh fading (BER)

The effect of Rayleigh fading is represented in Figure 3-9. It is assumed that there is only one path, and one finger for a Rake receiver. As the speed of user is increased, performance is poorer. As expected, Rayleigh fading severely impacts performance.

Only one path	# of fingers	# of users	SF	Speed of user
	1	3	16	100 km/h

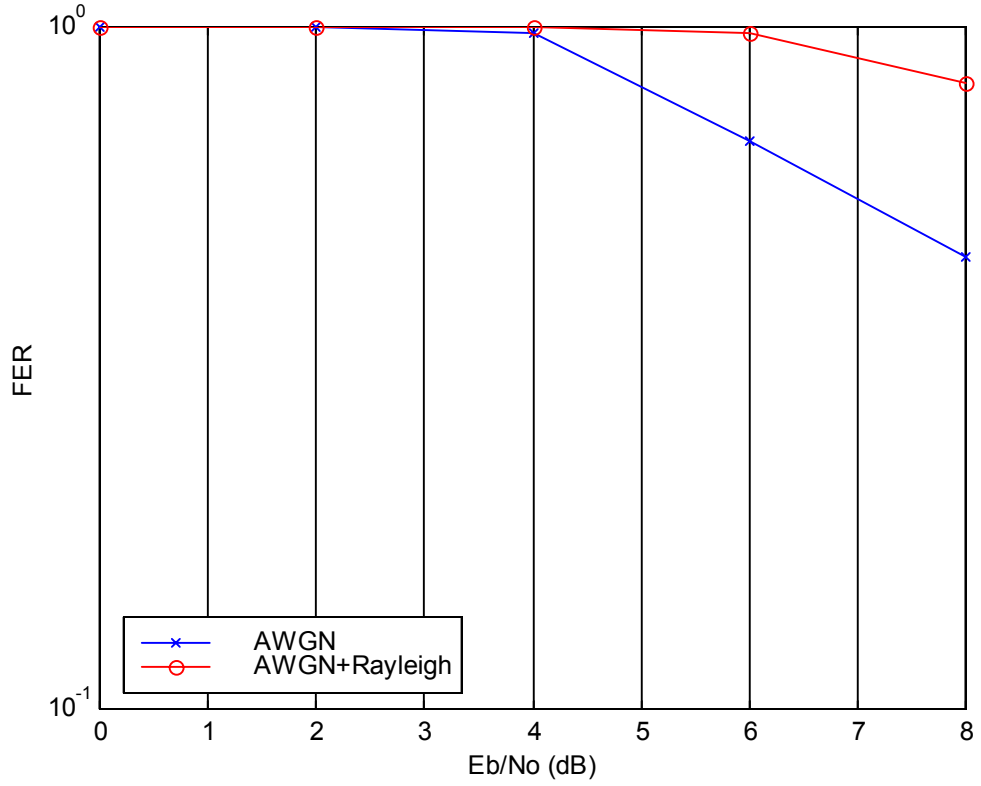

Figure 3-10. Effect of Rayleigh fading (FER)

In Figure 3-10, the effect of Rayleigh fading is represented in terms of FER. The frame length is the same as the length of 2560 chips. Since the performance in the Rayleigh fading channel poorer, the FER is higher.

Multipath fading	# of fingers	# of users	SF	Speed of user
	1	3	16	4 km/h

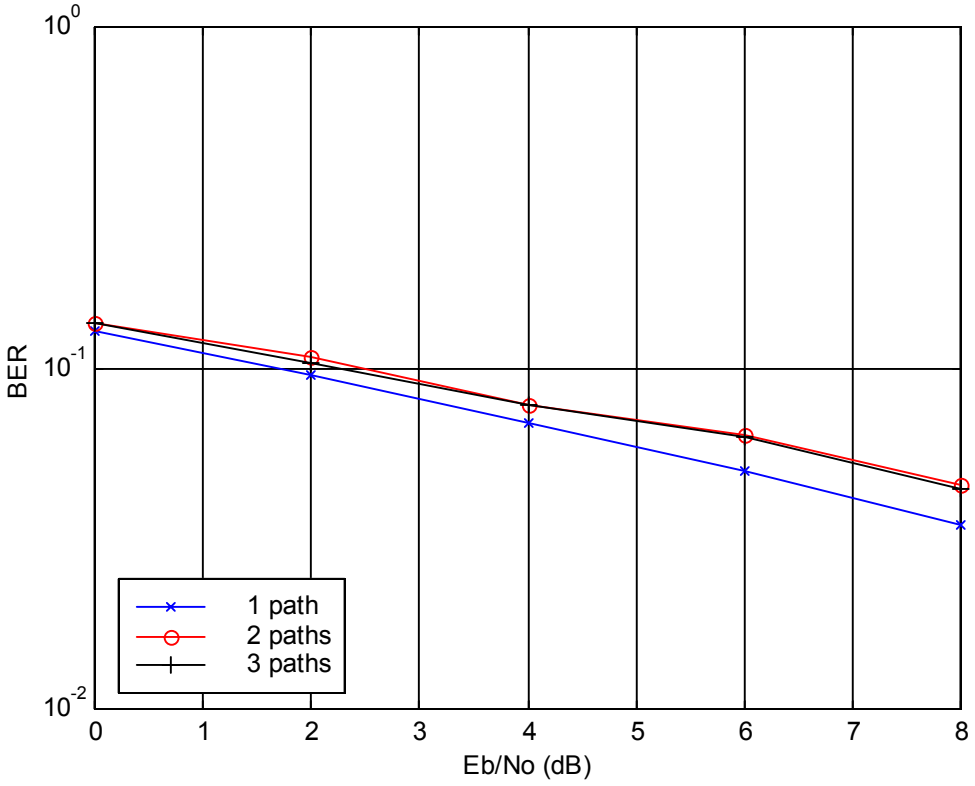

Figure 3-11. Different number of paths

For Figure 3-11, the number of Rake fingers is only one and the results explore the effect of multipath. Since only one finger is used, the receiver cannot resolve the signal components for the 2nd or 3rd path. Therefore, the more paths that exist, the more interference is caused. However, since the attenuation on 3rd path is severe according to Table 3-1, the 3rd-path signal almost does not cause interference.

SF	# of users	Speed of user
16	2	4 km/h

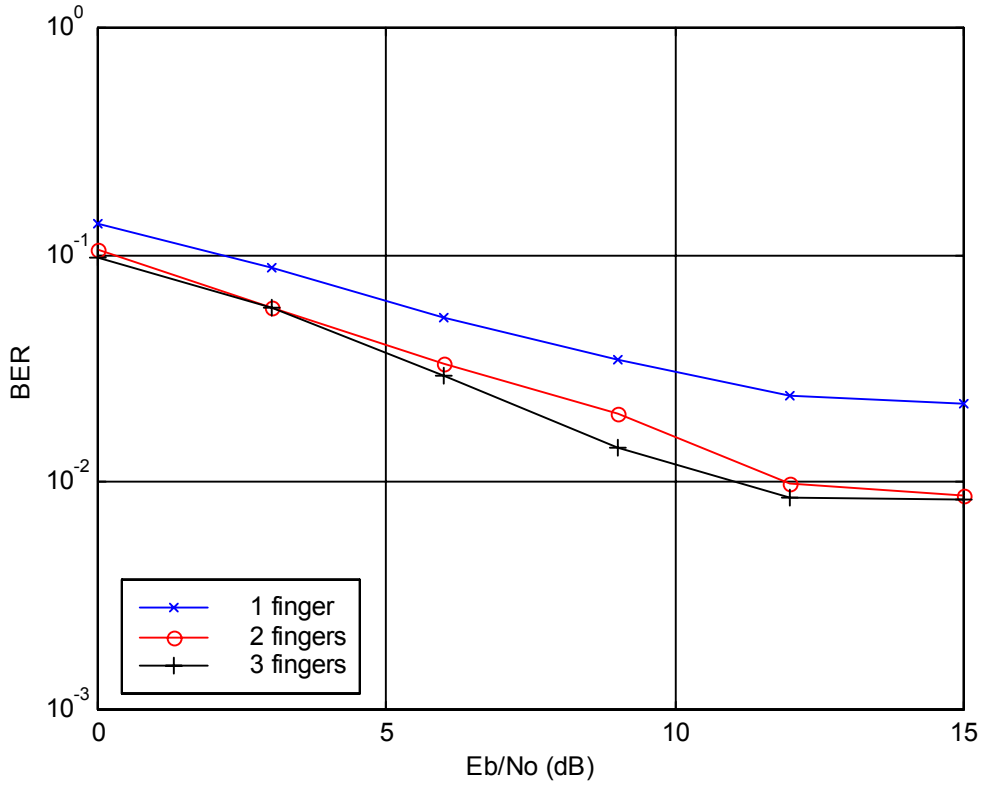

Figure 3-12. Different number of fingers of RAKE receiver

The more fingers of a Rake receiver that are used, the better the performance that can be expected since the additional fingers resolve multipath signal components. Figure 3-12 shows the performance changing according to various numbers of fingers. From Table 3-1, there are three paths which signals pass along with different time delays. As shown in Figure 3-12, the incremental performance improvement diminishes as the number of Rake fingers increases, owing the fact that less power is contained in additional multipath.

# of fingers	# of users	Speed of user
3	3	4 km/h

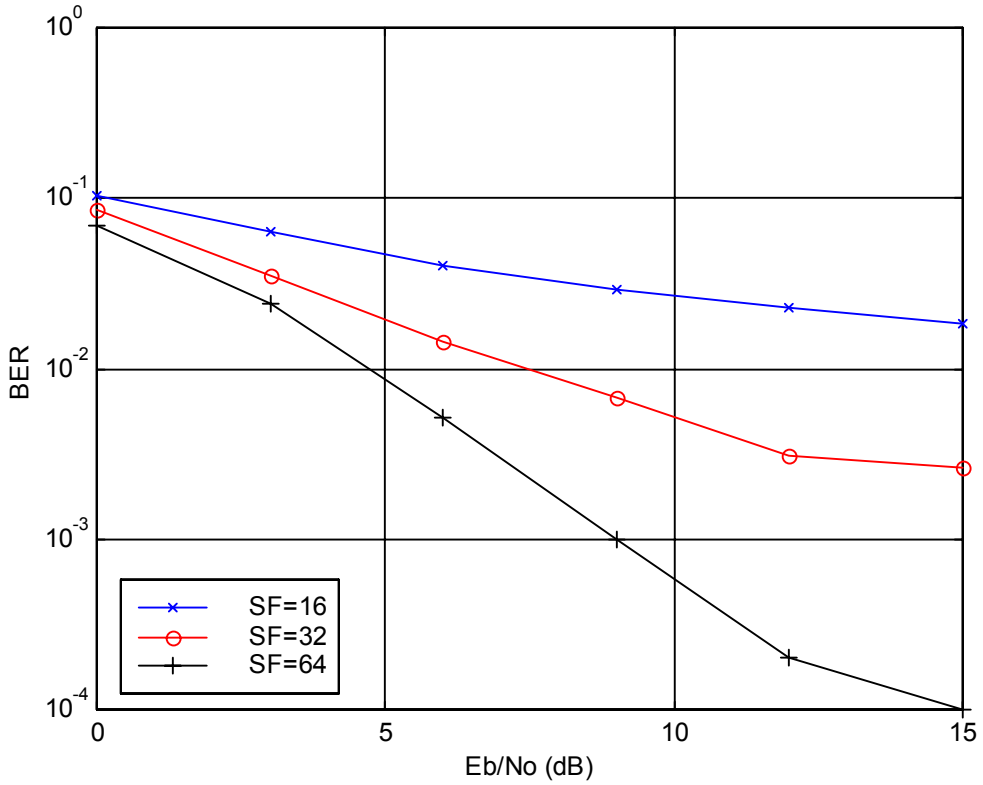

Figure 3-13. Different spreading factors

Figure 3-13 compares the performances at 16, 32 and 64 of spreading factor. The higher spreading factor is applied, the greater spreading gain can be guaranteed. However, since the increase of spreading factor is accompanied with the decrease of data rate, the choice of spreading factor is in accordance with a target BER or desired data rate.

# of fingers	SF	Speed of user
3	32	4 km/h

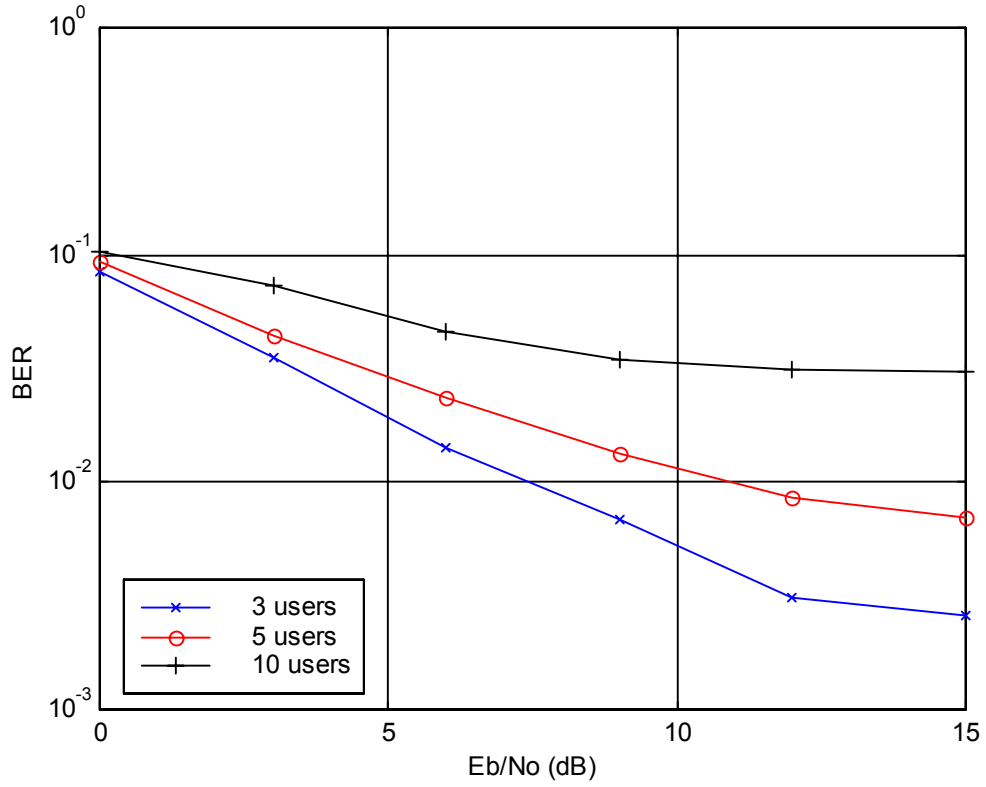

Figure 3-14 Different numbers of users

As described in Chapter 2, the other users' signals cause interference to a desired user. Therefore, there is an acceptable number of users to meet a desired QoS. As shown in Figure 3-14, when the number of users is 10, increasing the power of signal does not decrease the probability of bit error, creating on irreducible error floor. In order to preserve a desired QoS in the practical environment of changing number of users, some management processes should be performed: for example, increasing processing gain or blocking new users.

# of fingers	SF	# of users	Speed of user
3	32	3	4 km/h

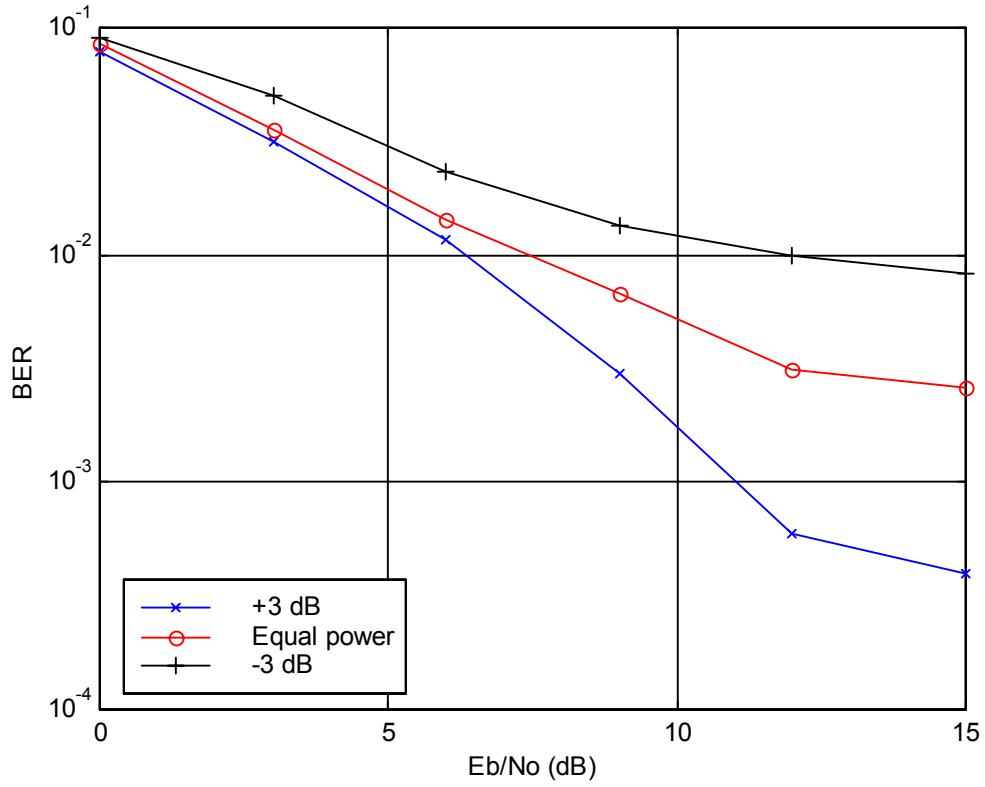

Figure 3-15 Different powers of desired signal

Increasing the power of a desired user's signal improves the performance of the desired user at the expense of other users experiencing more interference. In Figure 3-15, when the power of desired signal is 3dB higher than that of the other users' signals, the performance for desired user becomes better than the case of equal power. Conversely, when the power of desired signal is 3dB lower than that of the other users' signals, the performance for desired user becomes poorer than the case of equal power.

3.7. Chapter Summary

In this chapter, the implementation details of a simulation and simulation results are presented. The simulation model of AWGN and multipath fading channel, the property of OVSF codes, and the assumed data rate and bandwidth are described in Chapter 3. The simulation results show the effects of AWGN and multipath fading, and how the number of fingers or users, spreading factor, and signal power affect the performance.

Chapter 4. Hybrid coding with ARQ and FEC

This chapter presents the theoretical description of ARQ protocol, FEC scheme and hybrid coding. The purpose of this chapter is to represent the performance improvement with hybrid coding in theory and simulation.

4.1. Coding Scheme

In real wireless channel environment, noise and signal interference cause the desired signal to be easily harmed. Therefore, it is necessary to reduce the probability of bit error in order to meet quality of service requirements. Channel coding is one method for error detection and correction by means of adding redundant bits to information bits. In this section, the performance of block coding and convolution coding is investigated.

4.1.1 Block Codes

A block code is able to detect and correct error bits. In general, k information bits are represented as an n-bit code word through the encoding process. In other words, $n-k$ redundancy bits are added to obtain coding gain.

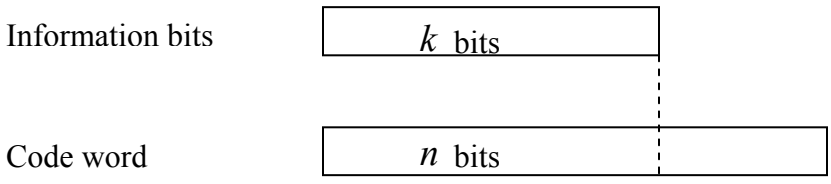

Figure 4-1. Code word

Usually, d and t denote error detection and correction capability, respectively. A lower bound on the required minimum distance to achieve a given error correction and detection capability is given by:

$$MD \geq t + d + 1$$
$$MD \geq 2t + 1$$
$$d > t,$$

where MD is the minimum distance.

If an error is inserted into the codeword by the channel, the receiver treats this situation in one of three ways. When the number of error bits contained in the code word is less or equal to t, the decoder detects and corrects the error bits. When the number of error bits is greater than t, and less or equal to d, the decoder just detects them and can not correct them. When the number of error bits is greater than d, the decoder cannot detect and accept the code word as a valid one. Thus, it is possible to use a block code to simultaneous detect and correct errors. In the examples to follow, we will focus on the case of a block code employed primarily for error detection.

There are two kinds of probabilities for receiving on erroneous code word after the error correcting procedure. One is the probability of a detected word error $P_d(E)$ and the other is the probability of undetected word error $P_u(E)$. They can be expressed as

$$P_d(E) = \sum_{i=t+1}^{d} A_i p^i (1-p)^{n-i} \tag{4-1}$$

$$P_u(E) = \sum_{i=d+1}^{n} A_i p^i (1-p)^{n-i} \tag{4-2}$$

where A_i : Number of code words of weight i;

p : Probability of a single bit error,

and n : Code length.

If the code's weight distribution is unknown, upper bounds on $P_d(E)$ and $P_u(E)$ can be obtained as

$$P_d(E) \le \sum_{i=t+1}^{d} \binom{n}{i} p^i (1-p)^{n-i} \tag{4-3}$$

$$P_u(E) \le \sum_{i=d+1}^{n} \binom{n}{i} p^i (1-p)^{n-i} \tag{4-4}$$

There is no chance to improve the probability of word error with undetected erroneous word. However, if an automatic-repeat-request (ARQ) protocol is used, the receiver can request a retransmission for a detected erroneous code word. This error control with a feedback channel improves the probability of word error as described in the following example.

Let us assume that n, t, d and p are 15, 0, 5 and 10^{-2} respectively.

i. No retransmission for a detected word error

$$P_d(E) \le \sum_{i=1}^{5} \binom{15}{i} \left(10^{-2}\right)^i \left(1-10^{-2}\right)^{15-i} \approx 0.1399 \tag{4-5}$$

$$P_u(E) \le \sum_{i=6}^{15} \binom{15}{i} \left(10^{-2}\right)^i \left(1-10^{-2}\right)^{15-i} \approx 4.6321\times10^{-9} \tag{4-6}$$

ii. One retransmission for a detected word error

$$P_{d,2}(E) = P_d(E)P_d(E) \le 0.0196 \tag{4-7}$$

$$P_{u,2}(E) = P_u(E) + P_d(E)P_u(E) \le 5.2804\times10^{-9} \tag{4-8}$$

iii. Two retransmissions for a detected word error

$$P_{d,2}(E) = P_d(E)P_d(E)P_d(E) \leq 0.0027 \tag{4-9}$$

$$P_{u,2}(E) = P_u(E) + P_d(E)P_u(E) + P_d(E)P_d(E)P_u(E) \leq 5.3711\times10^{-9} \tag{4-10}$$

From Equation (4-5) to (4-10), it can be shown that the ARQ protocol decreases the probability of word error.

$$P_d(E) + P_u(E) \quad > \quad P_{d,2}(E) + P_{u,2}(E) \quad > \quad P_{d,3}(E) + P_{u,3}(E) \tag{4-11}$$

Using an ARQ protocol, the general form of the probability of word error $P_w(E)$ can be written as

$$P_w(E) = P_{d,R+1}(E) + P_{u,R+1}(E) = \left(P_d(E)\right)^{R+1} + \sum_{j=0}^{R}\left(P_d(E)\right)^j P_u(E) \tag{4-12}$$

where the retransmission is conducted up to R times.

The word error rate can be translated into lower and upper bounds on the information-bit error rate. The lower bound is based on assuming that code word errors correspond to single information-bit errors in the corresponding message blocks. The upper bound is based on assuming that undetected word errors cause all of the decoded message bits to be incorrect. The upper bound is an approximation to $P_w(E)$ instead of an exact result [11]. The bounded bit error rate $P_b(E)$ can be expressed as

$$\frac{1}{k}P_w(E) \leq P_b(E) \leq P_w(E), \tag{4-13}$$

where k information bits are contained in one code word.

4.1.2 Convolutional Codes

Convolutional coding is different from block coding as an approach to error control. Convolutional coding is used for the forward-error-control (FEC) and a one-way error control scheme without feedback channel for retransmission request. Convolutional codes do not need to be constructed with a fixed code length. Information data passes through convolutional codes in a continuous stream [12]. When k_0 information bits are input into a convolutional encoder, n_0 coded bits result as output. The values of k_0 and n_0 are very small.

For example, assuming that k_0 and n_0 are 1 and 2 respectively, the encoder may be implemented as shown in Figure 4-2.

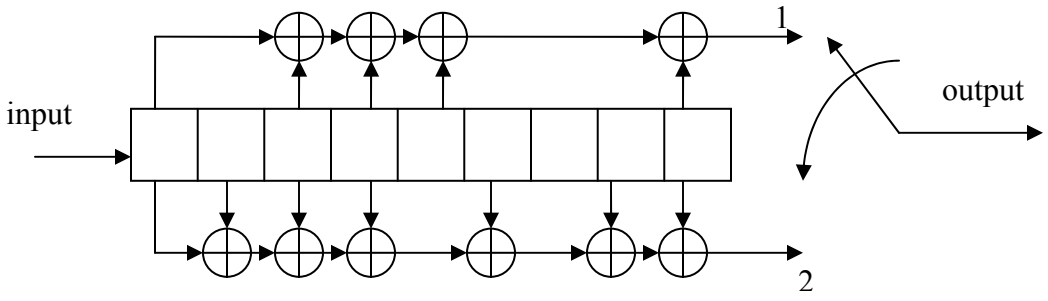

Figure 4-2. Convolutional encoder (G = [561, 753])

where the generator matrix G is [561, 753], indicating the location of the desired taps in a shift register. The constraint length K is the number of k_0-bit input sets which are contained in shift registers and have influence on the output. In Figure 4-2, the constraint length is 9 and the number of possible states is $2^{k_0(K-1)} = 2^8 = 256$.

The Viterbi algorithm is used for convolutional decoding. The minimum free Hamming distance d_{free} is the smallest Hamming distance separating any two distinct code sequences [12]. The performance of convolutional coding depends on d_{free}. The performance improves as d_{free} increases, but the complexity of decoder is directly proportional to the number of states 2^{K-1}.

Assuming that the hard-decision decoding is used, the pairwise probability of selecting a path at distance d from a correct path is expressed as

$$P_2(d) = \begin{cases} \sum_{k=\frac{d}{2}+1}^{d} \binom{d}{k} p^k (1-p)^{d-k} + \frac{1}{2}\binom{d}{\frac{1}{2}d} p^{d/2}(1-p)^{d/2}, & \text{if } d \text{ is even} \\ \sum_{k=(d+1)/2}^{d} \binom{d}{k} p^k (1-p)^{d-k}, & \text{if } d \text{ is odd} \end{cases} \quad (4\text{-}14)$$

where p is the probability of a bit error for the binary symmetric channel [12]. Using the Chernoff upper bound, $P_2(d)$ given in Equation (4-14) can be represented as

$$P_2(d) < \left[2\sqrt{p(1-p)}\right]^d. \quad (4\text{-}15)$$

The expression for the upper bound on the bit error probability is

$$P_b(E) < \sum_{d=d_{free}}^{\infty} B_d P_2(d), \quad (4\text{-}16)$$

$$P_b(E) < \sum_{d=d_{free}}^{\infty} B_d \left[2\sqrt{p(1-p)}\right]^d, \quad (4\text{-}17)$$

where B_d is the total number of non-zero information bits on all paths with weight d [16].

4.2. Simultaneous Use of Both of ARQ and FEC

In this section, we explore the combination of ARQ and FEC. According to the previous two sections, an ARQ protocol using block coding and an FEC scheme using convolutional coding both contribute to enhance the quality of data passed through an error-prone wireless channel. However, each of two methods follows a trade-off keeping for improving the performance. In case of the ARQ protocol, if the probability of a single-bit error p is high, retransmission does not lower the bit error rate steeply as shown in Figure 4-3. Also, an enormous number retransmissions can be required to obtain reasonable bit error rate, reduced the spectral efficiency of the system. Moreover, retransmissions increase the required time to transmit data.

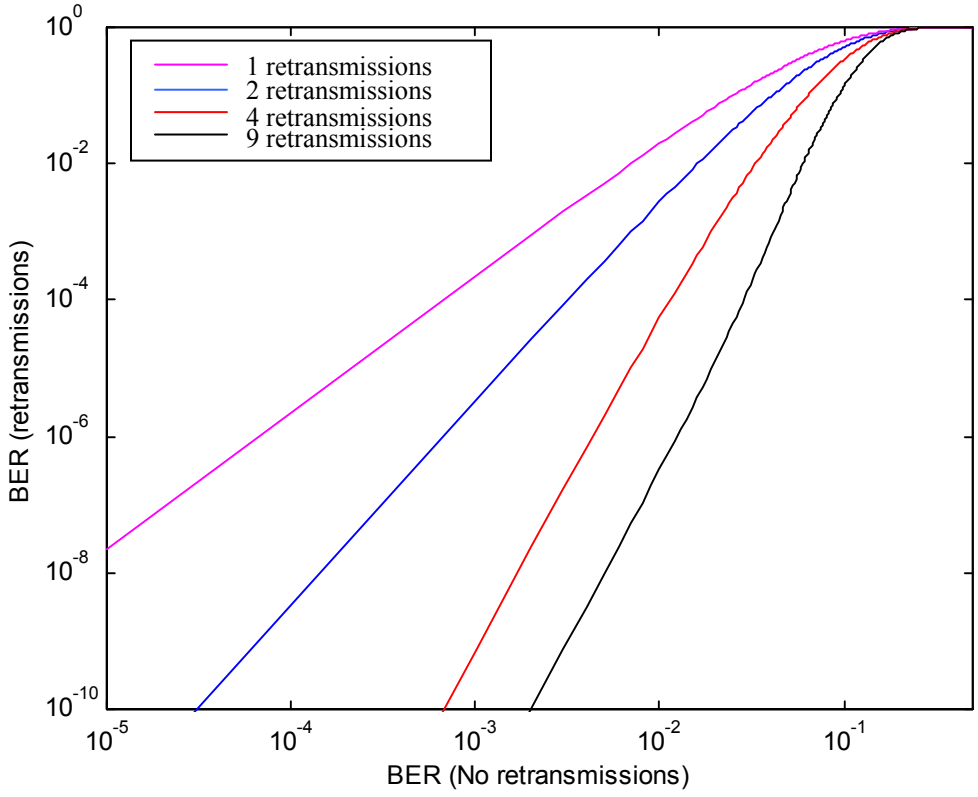

Figure 4-3. Upper bounds of ARQ protocol using BCH codes (15,7,5)

On the other hand, the performance of the FEC scheme is closely related to the complexity. The complexity of the Viterbi algorithm is proportional to the number of states 2^k which increases exponentially with the constraint length K [12]. As the Hamming free distance d_{free} becomes longer, the probability of selecting incorrect paths is decreased. Also, d_{free} is proportional to the constraint length K. Therefore, there is a trade-off between improving the performance of the FEC scheme and the corresponding complexity.

It is valuable to take into account the synergistic effect from using both the ARQ protocol and the FEC scheme. The block diagram in Figure 4-4 depicts how the two error-control techniques cooperate.

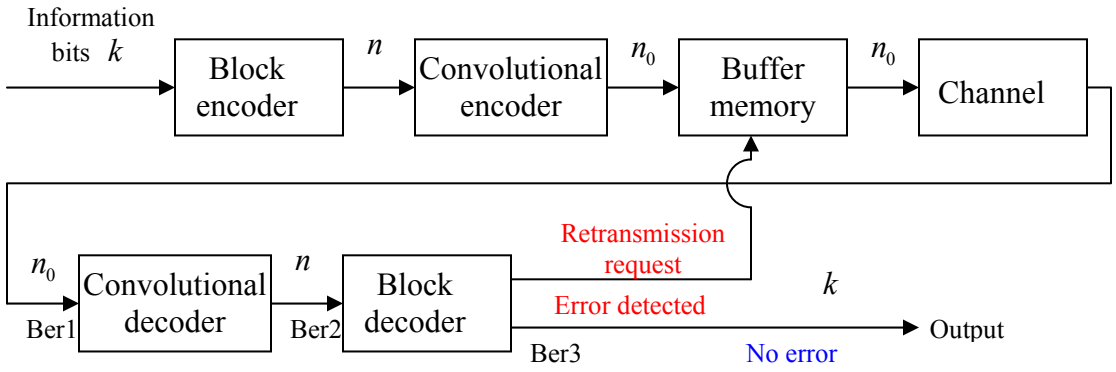

Figure 4-4. Flowchart for ARQ and FEC

In this system, the block coding scheme and the convolutional coding scheme play distinct roles in error control. In the beginning stage shown in Figure 4-4, k information bits are encoded to a n-bit block code. It is important to note that the data unit flowing through the diagram is a packet and the number of block codewords in a packet is

determined by packet size and chip rate. Assuming that B_p denotes the number of blocks contained in a packet, B_p block-code stream is encoded again by a convolutional encoder. At this point, the length of the convolutional code is $n_0 \times B_p$, and of course, it is shorter or equal to the packet size. The ultimate code word is described in Figure 4-5.

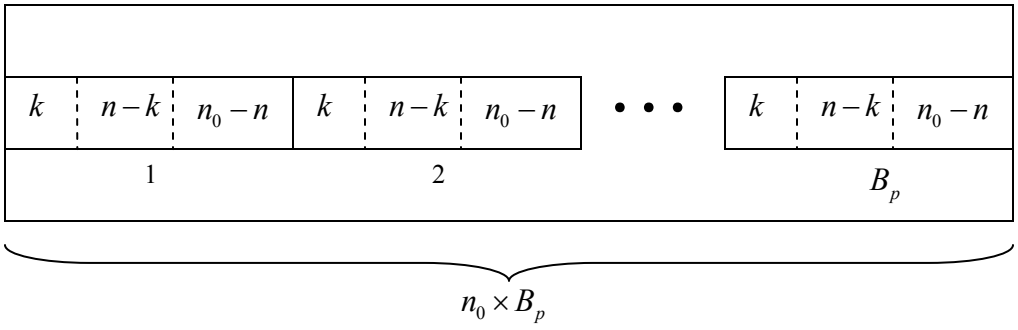

Figure 4-5. Code word after block and convolutional encoding

Each packet is transmitted to the receiver through channel, and is stored in the buffer memory until no erroneous block code is detected at the receiver. After a packet arrives at a receiver, convolutional decoding and block decoding are conducted in sequence. If any block code word is detected as an erroneous one, the receiver requests a retransmission for the packet to the transmitter. During the block decoding procedure for a retransmitted packet, it is needless work to repeatedly decode the blocks which have previously been detected as error free. Therefore, the block decoder should sort block codes to be decoded. That is described in Figure 4-6.

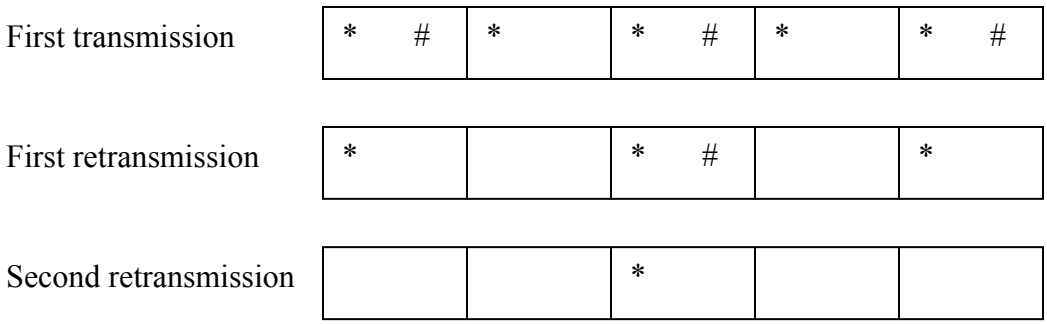

Figure 4-6. Block sorting for decoding
(* : Decoding is necessary, # : Errors are detected)

In Figure 4-6, the receiver will not request the third retransmission since no error is detected in the block codes from the second retransmission.

The performance enhancement can be presented from the perspective of the bit error rate. From Equation 4-3, 4-4, 4-13 and 4-17, the upper bound of the *ber*3 can be expressed as

$$ber3 \;<\; \left(P_d(E)\right)^{R+1} + \sum_{j=0}^{R} \left(P_d(E)\right)^j P_u(E) \tag{4-18}$$

where $P_d(E) \le \sum_{i=t+1}^{d} \binom{n}{i} (ber2)^i (1-ber2)^{n-i}$; (4-19)

$$P_u(E) \le \sum_{i=d+1}^{n} \binom{n}{i} (ber2)^i (1-ber2)^{n-i} , \tag{4-20}$$

and $$ber2 < \sum_{d=d_{free}}^{\infty} B_d \left[2\sqrt{ber1(1-ber1)} \right]^d . \tag{4-21}$$

In Figure 4.7, the probability of bit error in each case is shown; only ARQ, only FEC, and both of ARQ and FEC.

Another measurement of performance is FER (Frame Error Rate). If a receiver detects an erroneous frame which includes a bit error or bit errors, a retransmission is requested. The approximation of FER can be represented by

$$FER \approx 1-\left(1-P_w(E)\right)^{B_p} \tag{4-22}$$

where $P_w(E)$ is from Equation 4-12, and the required $P_d(E)$ and $P_u(E)$ are substituted with the upper bounds in Equation 4-19 and 4-20.

SF	# of users	# of fingers	Speed of user	ARQ	FEC
16	3	3	100 km/h	BCH code (15,7,5)	1/2 -rate convolutional code (G = [561, 753])

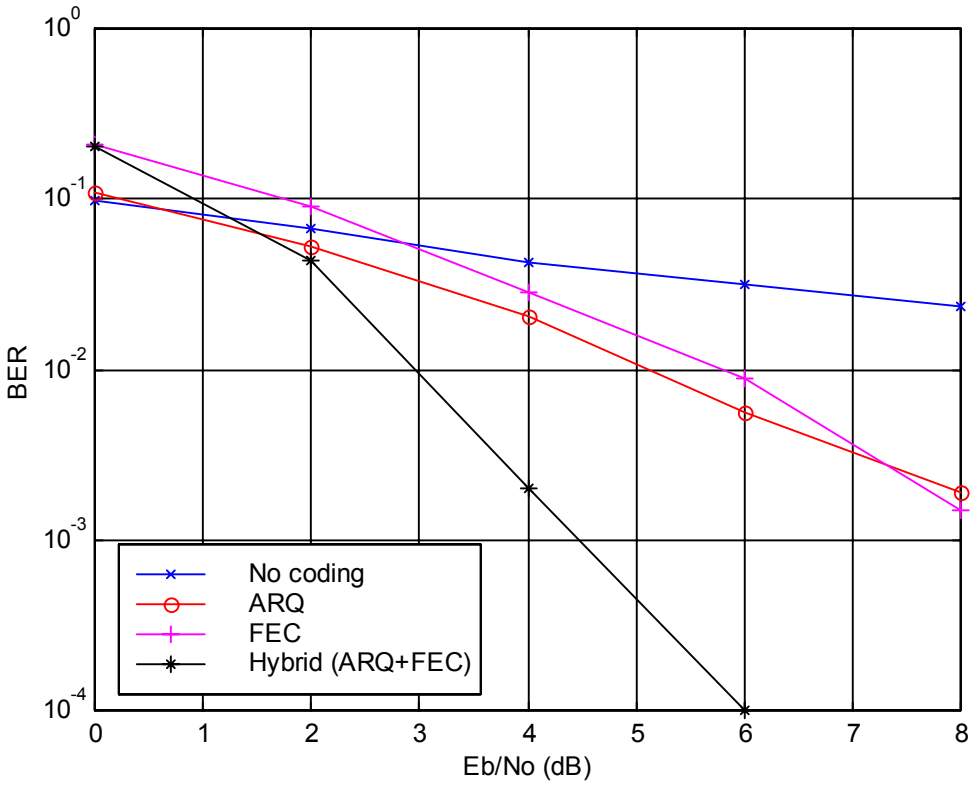

Figure 4-7. Comparison among ARQ, FEC, and ARQ+FEC (BER)

In Figure 4-7, the values of parameters are R=2, d=5, t=0, n=15, and d_{free}=12. R denotes how many retransmissions can be allowed for an erroneous packet. One packet contains 2560 chips. The CDMA system model for this simulation is the same as the one used in Chapter 3. The convolutional code of the generator matrix equal to [561, 753] is

used for the FEC scheme, and (15, 7, 5) BCH code is used for ARQ protocol. The retransmissions for an error-detected packet are made up to 2 times. As shown in Figure 4-7, the hybrid coding scheme significantly improves the performance. At 10^{-2} of BER, the hybrid coding scheme obtains between 2 and 3 dB more coding gain than either the ARQ protocol or FEC scheme by itself. Also, the resulting coding gain increases as the BER decreases.

SF	# of users	# of fingers	Speed of user	ARQ	FEC
16	3	3	100 km/h	BCH code (15,7,5)	1/2 -rate convolutional code (G = [561, 753])

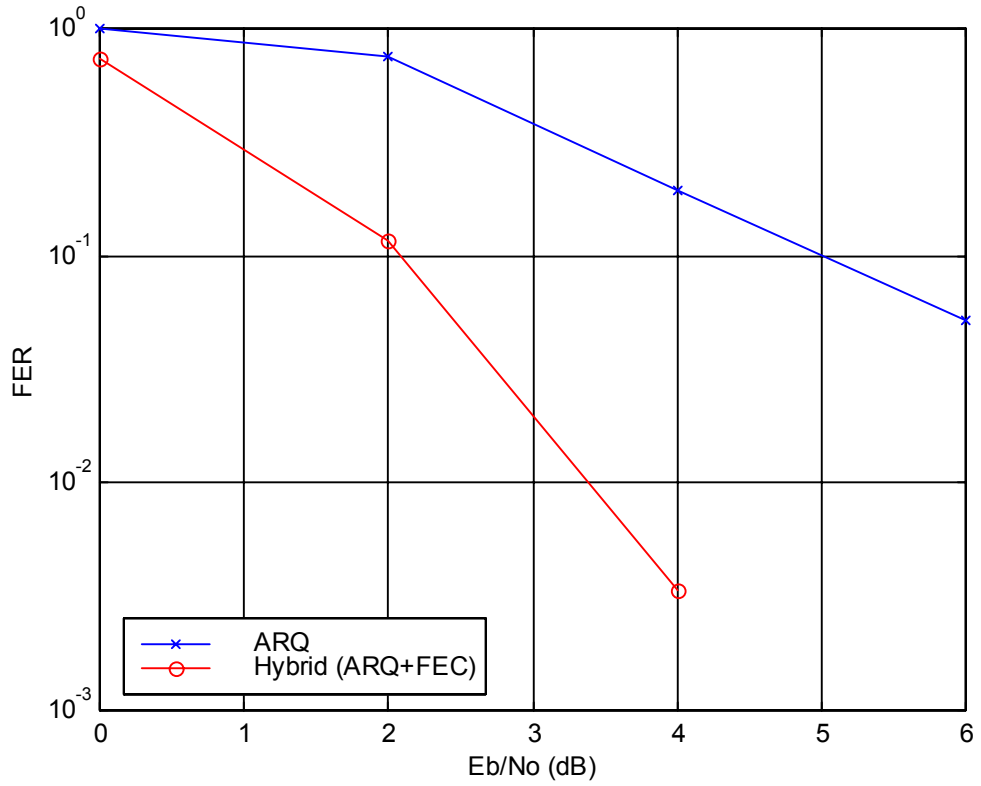

Figure 4-8. Comparison among ARQ and ARQ+FEC (FER)

Figure 4-8 shows the performance improvement of the hybrid coding scheme against ARQ protocol in terms of FER. In this simulation, one frame consists of 2560 chips, so 160 information bits are transmitted in one frame since the spreading factor is 16. As shown in Figure 4-8, since the FER of hybrid coding is lower than that of ARQ, the needed time for retransmissions is reduced in a system using hybrid coding.

# of users	# of fingers	Speed of user	No channel coding
3	3	100 km/h	

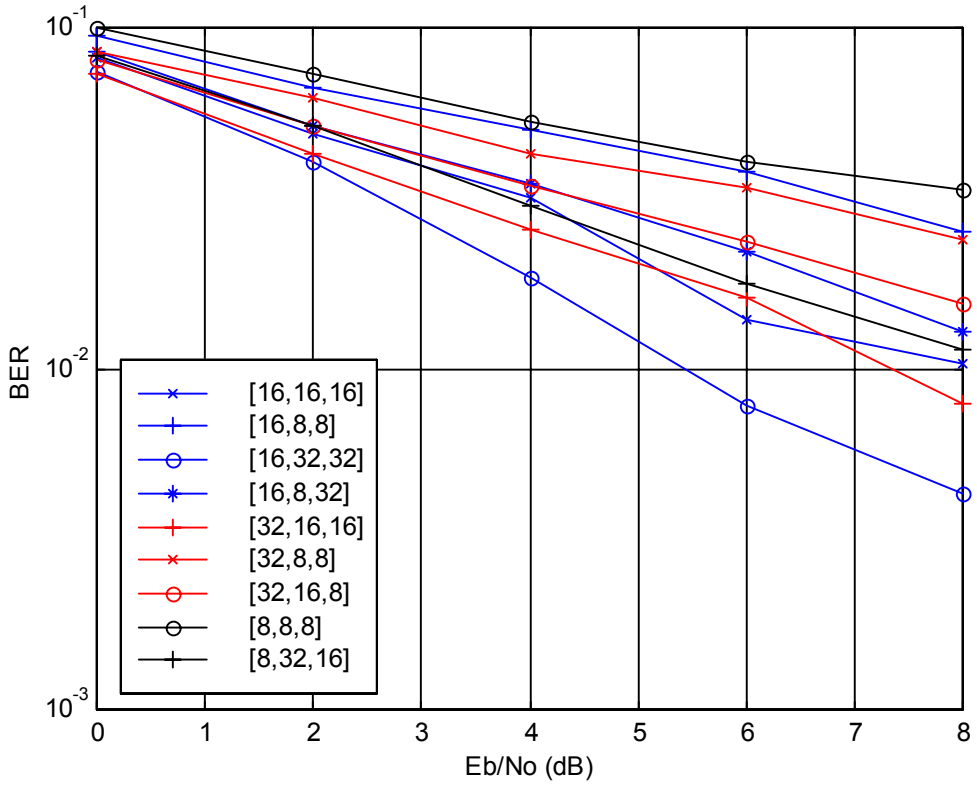

(a) BER

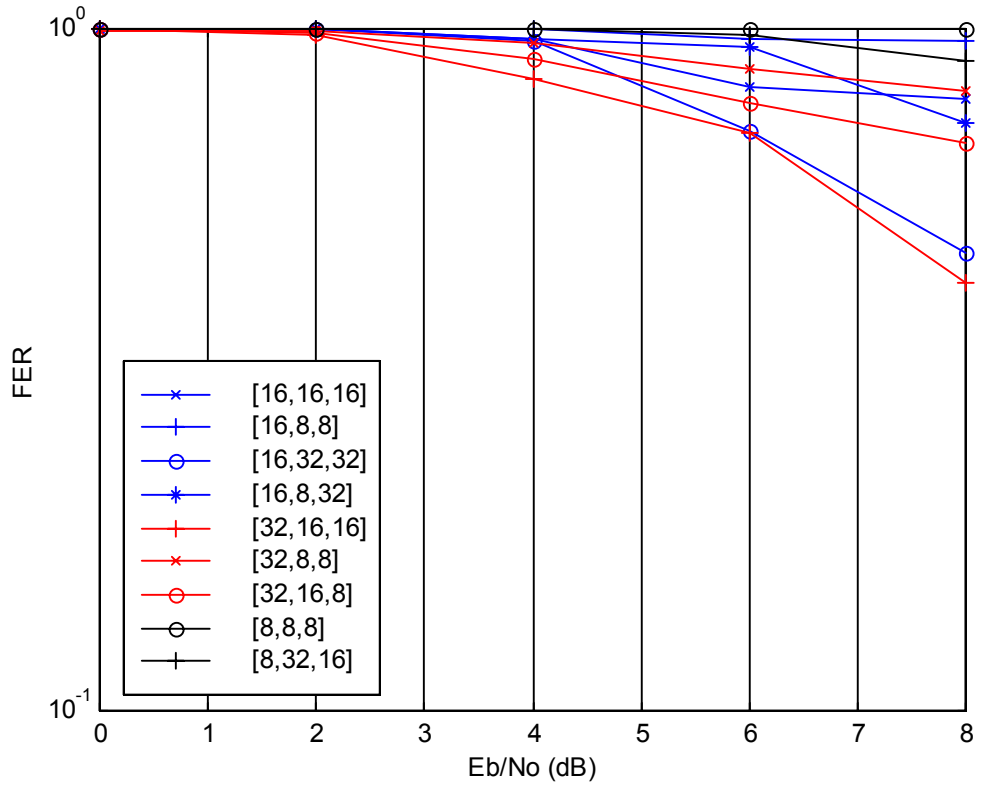

(b) FER

Figure 4-9. Performance of system with different processing gains (3 users)

In WCDMA system, various data classes with different spreading factors are supported. Therefore, it is necessary to scrutinize the performance in the case that the signals of concurrent users are spreaded by different factors. In Figure 4-9, there are nine different sets of SFs, and the sets are expressed in the following form.

$$[desired\ user,\ concurrent\ user\ 1,\ concurrent\ user\ 2]$$

The simulation results in Figure 4-9 show the performance of desired user. In this simulation, the energy per bit E_b is constant regardless of SF, and no channel coding scheme is employed. To increase data rate, the spreading factor of desired user is lowered.

However, reducing the SF causes the spreading gain to decrease, and the interference to other concurrent users is increased due to the stronger power of the desired user. In converse, as the SF of the desired user is increased, the interference to other users is reduced. As shown in figure 4-9(a), the performance of [16, 32, 32] is better than that of [16, 16, 16] since the increase of SFs for other concurrent users means the decrease of interference to desired user.

In the comparison of [8, 32, 16], [16, 8, 32] and [32, 16, 8], each of the three users has different SF, and the user with the SF of 8 shows the best performance. In this situation, the signal power enhancement dominates over the spreading gain increase.

# of users	# of fingers	Speed of user	ARQ
3	3	100 km/h	(15,7,5) BCH code

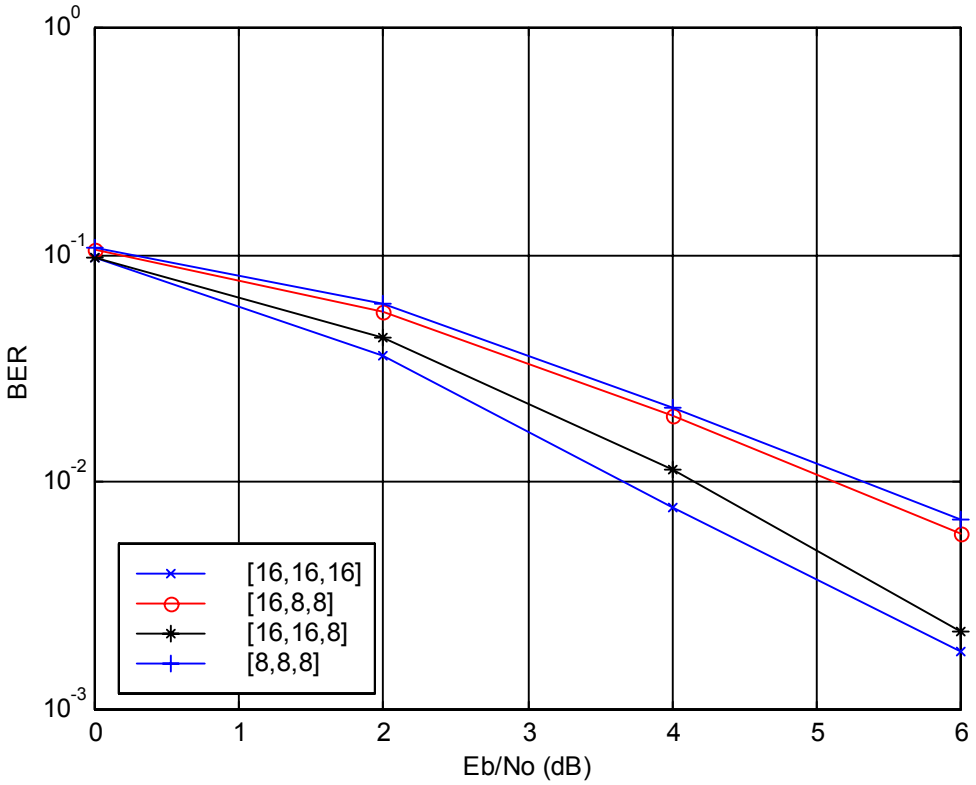

Figure 4-10 (a): BERs for users with different spreading factors using ARQ protocol.

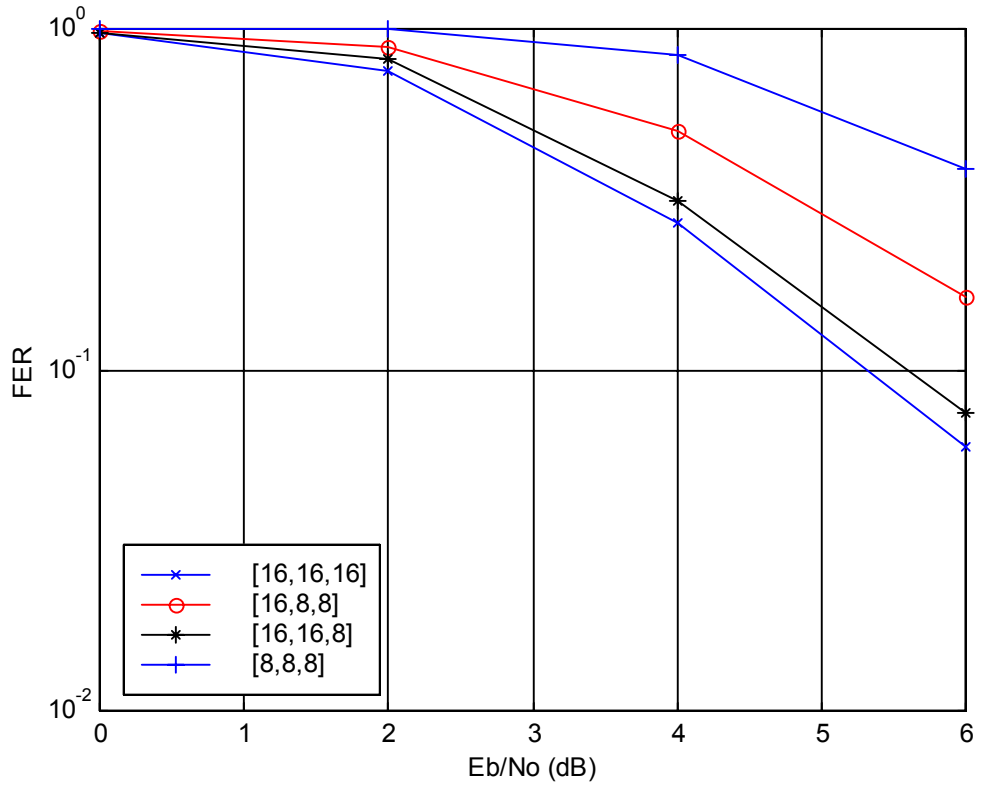

Figure 4-10 (b): FERs of users with different spreading factors using ARQ protocol.

Figure 4-10 shows the simulation results for an ARQ protocol applied to users with different SFs. For erroneous packets, retransmission is requested up to 2 times. The performance of [16, 16, 16] is better than that of [16, 16, 8] or [16, 8, 8] since the lower SF of the concurrent users causes more interference to desired user.

# of users	# of fingers	Speed of user	Hybrid Channel coding	
			ARQ	FEC
3	3	100 km/h	BCH code (15,7,5)	1/2 -rate convolutional code (G = [561, 753])

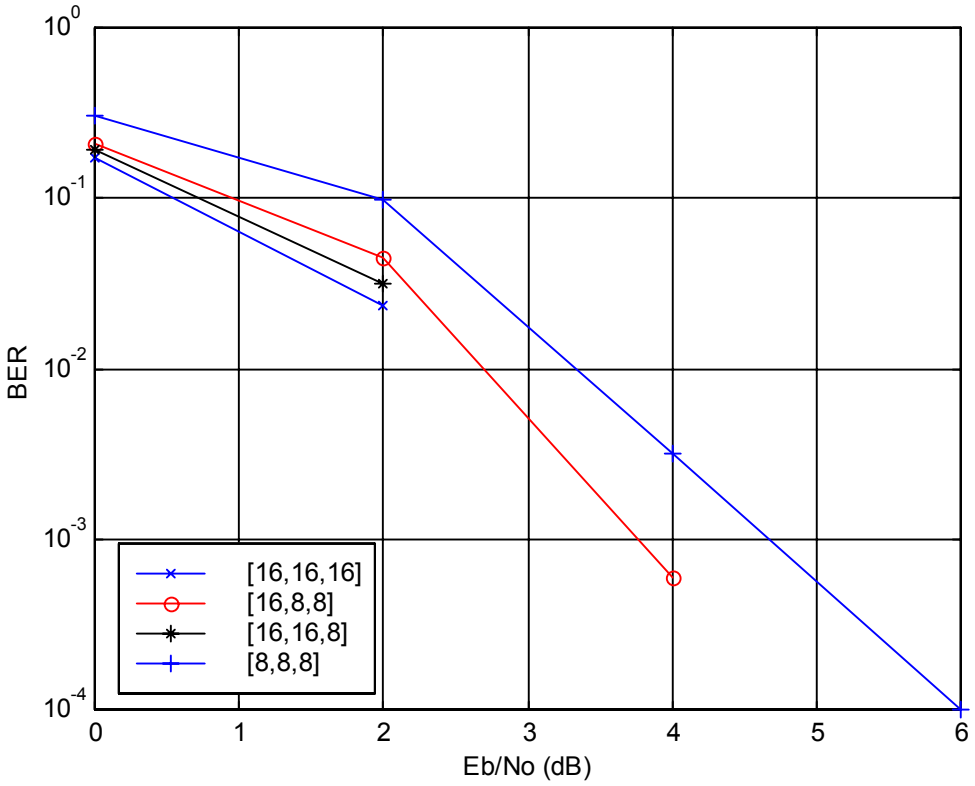

Figure 4-11 (a): BER vs. E_b/N_0 for users with different SFs, using the hybrid ARQ scheme.

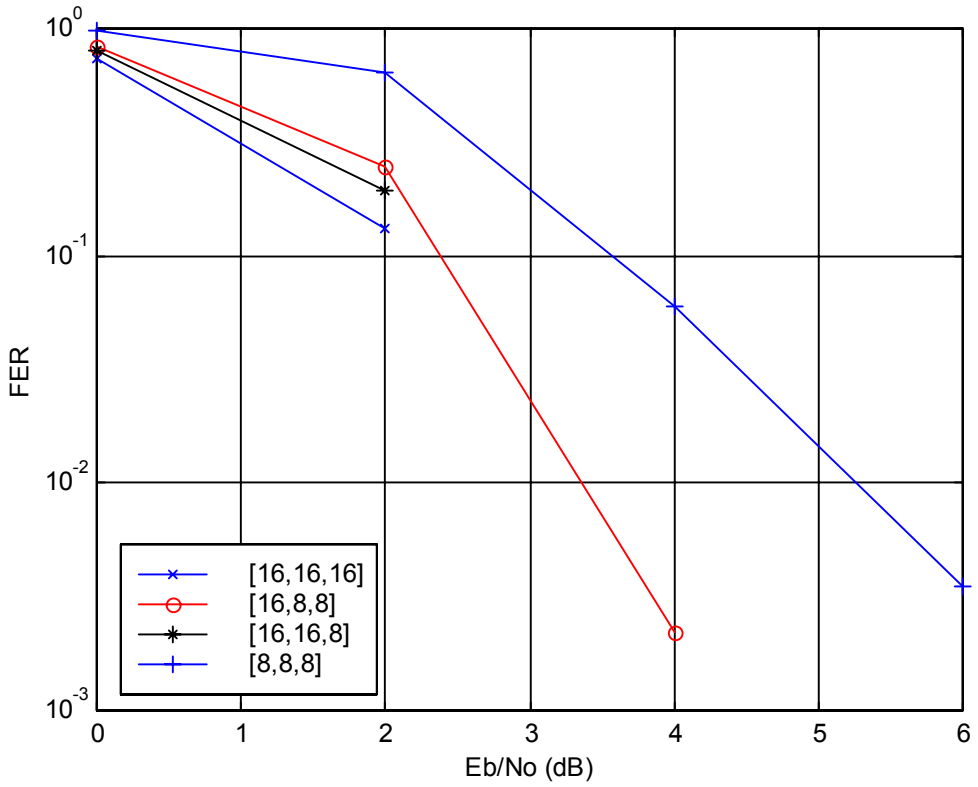

Figure 4-11 (b): FER vs. Eb/No for users with different SFs, using the proposed hybrid coding/ARQ scheme.

Figure 4-11(a) and 4-11(b) show that using the proposed hybrid channel coding/ARQ scheme, the performance improves dramatically for BER and FER, respectively. As before, reduction of SFs causes increased interference to other users in the system, leading to decreased performance levels. In Figure 4-11, the resolution of the simulation results is poor in some cases due to the required simulation time.

4.3. Chapter Summary

This chapter shows that a hybrid FEC/ARQ scheme can significantly enhance the performance of a DS-CDMA system. The BER and FER was derived in mathematical form and obtained by computer simulations. The impact of different SFs for concurrent users was investigated.

Chapter 5. Conclusion and Future Work

5.1. Conclusion

This thesis presents a mathematical description of CDMA systems, a simulation embodiment and a hybrid coding technique. In Chapter 2, the desired signals, interference and noise component of DS-CDMA were mathematically analyzed under the conditions of a frequency selective channel. RAKE receiver can gather dispersed desired signals on multipath channel. As shown in Figure 3-7, the more fingers of a RAKE receiver that are used, the lower bit error rate that can be expected. It is important to note that the performance of a RAKE receiver depends on channel environment. If the power of multipath signals is heavily attenuated, the bit error rate is increased. All the simulation results of this thesis are based on the power delay profile in Table 3-1, which reflects an urban microcell case. Interference is caused by other users and other multipath components. The simulations of uplink and downlink are different in the aspect of the synchronicity of combined signals. In uplink, each user transmits signals from random time point, so all users' signals are combined asynchronously. On the other hand, in downlink, all signals are transmitted by one base station, so they are combined synchronously. In this thesis, simulation results presented focus on the uplink. For computer simulation, AWGN samples and Rayleigh fading waveforms should be generated as described in Chapter 3.

The kernel of this thesis is included in Chapter 4. As mentioned in the introduction part, this thesis is focused on the use of hybrid channel coding to enhance the data performance of a CDMA network. Coding schemes can be applied for error

detection and correction. An ARQ protocol is enabled by error detection capability and a FEC scheme requires error correction capability. Block coding can be used for both error detection and correction. However, it is restricted to error detection in this thesis. Several block coding schemes are developed up to now. A (15, 7, 5) BCH code is used for the simulation. Convolutional coding is for error correction using the Viterbi algorithm. ½ - rate convolutional code with generator matrix [561, 753] is used for the simulation. As shown in Figure 4-4, the FEC scheme corrects error bits before requesting erroneous code words. After error correction procedure by the convolutional decoding, still detectable erroneous code words are found by the block decoding. When an erroneous code word is detected, a retransmission is requested up to R times per packet. According to Equation 4-11, retransmitted code words have smaller word error probability than first transmitted code words. Eventually, the bit error rate decreases faster than that of single use of ARQ protocol or FEC scheme as shown in Figure 4-7.

5.2. Future Work

The research on this thesis is intended to study a hybrid coding scheme for ARQ protocol and FEC. Including BCH code, there are many other block coding schemes such as Hamming code, cyclic code and Reed-Solomon code. In the future, we would like to simulate the various combinations of block codes and more powerful error correction scheme like Turbo codes. Also, TCM (Trellis-Coded Modulation) scheme could be another choice for FEC in aspect of bandwidth efficiency.

The selection of modulation scheme affects the performance of a cellular communications system. Also, the spreading factor in WCDMA is variable. Therefore,

error detection scheme, error correction scheme, modulation scheme and spreading factor are the parameters which can determine the QoS of a traffic class in Table 1-1. Each of the traffic classes has different tolerance limits for error-sensitivity and delay-sensitivity. So, assuming that the parameters are adaptable within a CDMA system, it is necessary to optimize the parameters according to the required QoS of corresponding traffic class or application. The study about such an optimization algorithm can be an extended research from this thesis. Also, HSDPA (High-Speed Downlink Packet Access) and AMC (Adaptive Modulation and Coding) can be ultimate research fields starting from this thesis.

References

[1] Jens Zander and Seong-Lyun Kim, “Radio Resource Management for Wireless Networks”, 2001, Artech House Publishers.

[2] Tero Ojanpera and Ramjee Prasad, “WCDMA: Towards IP Mobility and Mobile Internet”, 2001, Artech House Publishers.

[3] Walter Tuttlebee, “Software Defined Radio – Origins, Drivers and International Perspectives”, 2002, Wiley.

[4] Ulrich Rohde and Jerry Whitaker, “Communications Receivers – DSP, Software Radios, and Design, 3rd edition”, 2001, McGRAW-HILL.

[5] Nishith D. Tripathi, Jeffrey H. Reed, and Hugh F. VanLandingham, “Radio Resource Management in Cellular Systems”, 2001, Kluwer Academic Publishers.

[6] Andrew J. Viterbi, “CDMA Principles of Spread Spectrum Communication”, 1995, Addison-Wesley.

[7] Theodore S. Rappaport, “Wireless Communications – Principles and Practice”, 1996, Prentice Hall PTR.

[8] Stavros Striglis, “A Multistage RAKE Receiver for CDMA Systems”, 1994, MS Thesis, Virginia Tech.

[9] Francis Swarts, Pieter van Rooyan, Ian Oppermann and Michiel P. Lotter, “CDMA Tachniques for Third Generation Mobile Systems”, 1999, Kluwer Academic Publishers.

[10] Byeong Gi Lee and Byoung-Hoon Kim, "Scrambling Techniques for CDMA communications", Kluwer Academic Publishers, 2001.

[11] Stephen B. Wicker, "Error Control Systems for Digital Communication and Storage", 1995, Prentice Hall.

[12] Michael Buehrer, "Lecture notes – Digital Communication (ECE 5654)", Spring 2002.

[13] Yingbo Li and Y.L. Guan, "Modified Jakes' Model for Simulating Multiple Uncorrelated Fading Waveforms", IEEE Vehicular Technology Conference Proceedings, VTC 2000 Tokyo, IEEE 51st, Vol. 3, pp. 1819-1822, Spring 2000.

[14] Harri Holma and Antti Toskala, "WCDMA for UMTS – Radio Access for Third Generation Mobile Communications, second edition", 2002, Wiley.

[15] V.R. de Carvalho and C. de Almeida, "Capacity analysis of an ARQ scheme for multimedia DS-CDMA systems", IEE Proceedings - Communications, Vol. 147, Issue : 4, pp. 201-204, August 2000.

[16] John G. Proakis, "Digital communications, fourth edition", 2001, McGraw-Hill Higher Education.

[17] John G. Proakis and Masoud Salehi, "Contemporary Communication Systems using MATLAB", 2000, Brooks/Cole Thomson Learning.

VITA

Byungwan Yu received his undergraduate degree in School of Electrical and Electronics Engineering, in Febrary, 2001, from Chung-Ang university, Seoul, South Korea. After completing his undergraduate education, he started in the M.S. program at Virginia Tech from the fall of 2001 and joined MPRG in the summer of 2002. His research interests include Channel Coding Schemes and Radio Resource Management for WCDMA systems. He did his internship in Samsung Electronics Co. during the summer of 2003. He worked on the algorithms used in Radio Resource Management for WCDMA systems during the internship program. He is supposed to work in Telecommunication Network Division of Samsung Electronics Co. from October, 2003.